Chapter 3

Semiconductor Optical Amplifier for Next Generation of High Data Rate Optical Packet-Switched Networks

Guilhem de Valicourt, Miquel Angel Mestre Adrover, Nikolay D. Moroz and Yvan Pointurier

Additional information is available at the end of the chapter

http://dx.doi.org/10.5772/61990

Abstract

This chapter provides an overview of considerations for the development of semiconductor optical amplifiers (SOA) for the next generations of packet-switched optical networks. SOA devices are suitable candidates in order to realize high-performance optical gates due to their high extinction ratio and fast switching time. However such devices also introduce linear and nonlinear noise. The impact of SOA devices on several modulation formats via theoretical model, numerical simulation, and experimental validation is studied. Impairments introduced by SOAs are considered in order to derive some general network design rules.

Keywords: Semiconductor optical amplifier, optical packet-switched network, coherent communications, network design rules

1. Introduction

Since 2010, coherent technology has paved the way toward high-capacity optical communications [1]. Coherent systems allow transmitting information with multi-level modulation formats over both polarizations [polarization division multiplexing (PDM)] of light, which increases the spectral efficiency [bit/s/Hz (b/s/Hz)] while relaxing the need for ultrahigh symbol rates to achieve data rates beyond 100 Gb/s. Such technology is enabled by fast analog-to-digital and digital-to-analog converters (ADC and DAC), which, together with coherent receivers and robust digital signal processing (DSP), allow for the generation and recovery of advanced modulation formats. PDM-quadrature phase-shift keying (QPSK) and PDM-16-quadrature amplitude modulation (QAM) signaling at 28 or 32 Gbaud are currently used to develop 100 and 200 Gb/s transponders used in today's core networks. However, experimental

results showing interfaces transmitting beyond 400 Gb/s [2] and up to 1 Tb/s [3] have already been demonstrated. At present, coherent systems are mainly present in long haul systems. However, a huge traffic growth (up to 560% in 5 years) is expected by 2017 in metropolitan optical networks [4]. In addition, data centers' global traffic presents a relentless growth, with 75% of such traffic flowing within data centers. The overall need of capacity together with the drop expected in coherent transponders' cost makes evident the expansion of coherent systems toward other network segments.

Furthermore, the ever-emerging bandwidth-on-demand services in optical fiber networks induce distributed and bursty traffic profiles. Network flexibility and high efficiency are then required to handle these new traffic characteristics. Hybrid time/wavelength division multiplexing (TDM /WDM) systems could be the right trade-off between the high capacity provided by the WDM virtual point-to-point links and the TDM sub-wavelength switching granularity, allowing very efficient systems. Therefore, the WDM optical packet-switched network was proposed to unite these benefits and reduce the power consumption compared to circuit-based networks [5]. Ring nodes collect and aggregate the traffic from the access segment, into fixed-duration optical packets and relay them to a WDM synchronous optical packet-ring network. Asynchronous and variable-size internet protocol (IP) packets that can be as small as 40 bytes are too short at high data rates (10 Gb/s in access networks, 100 Gb/s and above in metro/core transport networks) to be efficiently switched with current optical technologies. To resolve this problem, packets are first aggregated at the network edges into "bursts" (here, slots) of data, which are sufficiently long to be compatible with the switching times of optical elements. Furthermore, synchronous switching of continuous streams of optical slots is preferred because it allows straightforward reuse of conventional erbium-doped fiber amplifiers (EDFAs).

These ring nodes also provide optical transparency for the optical slots in transit and add/drop/blocking capabilities at the slot granularity thanks to optical logic gates or slot blocker (SB) devices [6]. SB devices are advantageous for increasing network efficiency, by erasing or transmitting the upcoming optical slots, enabling spatial reuse of the wavelengths. A slot blocker structure consists of a wavelength demultiplexer, one optical gate per wavelength enabling the structure to selectively erase any slot, and a wavelength multiplexer. The optical gate is one of the most crucial elements of the node as it is responsible for the (optical) quality of the transiting slots, and optical gate specifications, such as high extinction ratios above 25 dB, large optical bandwidth (over the C-band), and switching times between pass and block states below 30 ns are typically required. Colorless optical gates, such as Mach–Zehnder modulators (MZM), electro-absorption modulators (EAM), variable optical attenuators (VOA), or semiconductor optical amplifiers (SOA), are considered as potential candidates for the SB structure. Providing a cost-efficient approach, such devices have been proposed in the silicon platform as key building blocks for the fast SB as MZM [7], ring resonator structure [8], or VOA based on p–i–n carrier-injection structures [9]. However, MZM or ring resonators exhibit low extinction ratios (< 15 dB), like the previous type of VOA when utilized for short switching time (< 15 ns). More recently, silicon-on-insulator (SOI)-based monolithically integrated slot-blocker integrating the multiplexer and demultiplexer as well as all optical gates was proposed in a two-port/one-port package and for single/dual polarization [10–11].

http://dx.doi.org/10.5772/61990

However, active devices are expected to offer higher extinction ratio and faster switching time along with a reduction of the insertion loss, thus avoiding the use of extra optical amplifiers as well as allowing fast power equalization providing the guarantee of error-free transmission over a large cascade of optical nodes. EAMs have also been investigated as they provide fast switching time. However, the wavelength-dependent optical losses limit the spectral operation range, and more complex structures are needed, which require the integration of EAM and SOA into a single chip [12]. The large optical bandwidth, high extinction ratio, high gain, and fast switching time make SOA more suitable candidates. Despite the development of SOA devices having a sluggish start compared to that of fiber amplifiers for in-line amplification, the recent progress in optical semiconductor fabrication techniques and device design has pushed the performance of SOAs well beyond the state of the art. SOAs promise to take a key role in the evolution of optical packet-switched networks. Furthermore, in order to drive down the cost of the SB, several approaches derived from the SOA technology have been proposed, for example, using low-cost optical gate, such as reflective SOA (RSOA) devices, designed for access network [13] or hybrid III–V on silicon optical gate array [14]. However, SOA devices, being suitable candidates as optical gate, also bring limitations on optical signal reach. The addition of amplified spontaneous emission (ASE) noise degrades the optical signal-to-noise ratio (OSNR). Their nonlinear behavior causes self-phase modulation (SPM) (when operating with single channel) translating in nonlinear phase noise. Both effects degrade signal quality and increase the bit error rate (BER). Such impairments might become critical in optical networks and even more in coherent systems where information is transmitted in both amplitude and phase of the optical signal. Therefore, novel network design rules need to be considered when introducing SOA-based optical nodes.

This chapter discusses the general context of slot-switched network with possible slot blocker implementation in Section 2 and focuses on SOA devices in Section 3. First, we present the evolution of SOA with the development of optical communication systems. The level of knowledge and development on this technology as well as a comprehensive introduction of SOA devices are described. Then, we study the impact of SOA devices of optical signals carrying data information. To do so, the impact on different modulation formats, such as on–off keying (OOK), QPSK and QAM, is explained and modeled via analytic and numerical simulations. Finally, SOA-based network design focusing on specific issues related to the linear and nonlinear noise from the SOA is presented in Section 4. We evaluate the final performance of a large cascade of SOAs and assess novel design rules based on the accumulation of nonlinear distortions.

2. Toward Optical Packet-Switched Networks

2.1. Advantages of Packet Switching

2.1.1. Optical circuit switching

Optical circuit switching (OCS) has become the *de facto* basic standard technology underlying backbone networks since the early 2000s. With OCS, a permanent connection called "light-

path" is statically allocated from end to end. The connection is mapped to one or several wavelengths, which are dedicated to the connection. Optical circuits can traverse nodes called optical cross-connects (OXC) or reconfigurable optical add-drop multiplexers (ROADM) "transparently," that is, without costly and energy-consuming conversions between the optical and the electrical domains, and without processing in the electrical domain, such as electronic switching. Typically, OCS networks are dimensioned for the peak demand for each connection; when demands are relatively constant with time, as is the case in backbone networks where many demands are aggregated, such provisioning is efficient and wastes little capacity. In addition, OCS suffers from the so-called N^2 scalability issue: in a network of N nodes where demands are highly meshed and all or most nodes need to interact with all or most of the other nodes, the required number of circuits grows as N^2, which can quickly exhaust the limited number of available wavelengths (typically, 80–96) available in the transmission C-band on an optical fiber. OCS networks are static; they are not meant to be reconfigured faster than the second or millisecond timescale, and are typically reconfigured at much lower speeds.

For instance, Figure 1(a) depicts a six-node network with channel data rate of 100 Gb/s. Nodes consist of transponders (transmitters, TX; and receivers, RX) statically mapped to predetermined colors and an optical switching fabric that is slow reconfigurable, such that the network itself is slow reconfigurable, as mentioned above. All four (peak) demands, 75 Gb/s from A to C, 25 Gb/s from A to D, 100 Gb/s from A to E, and 50 Gb/s from B to D, are routed in the optical domain, with no optoelectronic conversion. As three demands originate from node A, three transponders are needed at node A. A full 100 Gb/s wavelength is dedicated to the demand between A and D, meaning that 75% of the allocated capacity is wasted for this 25 Gb/s demand. Due to this waste, two wavelengths are needed between A and B (and also between B and D). It was observed that, due to optical transparency, the demand between A and E transits transparently through intermediate node F, which only requires an optical switching fabric, but no transponder.

2.1.2. Electronic packet switching

In segments closer to the end user, such as metro networks or data centers, demands between the users may not be constant, and allocating circuits for the peak demand becomes inefficient and wastes network capacity. In such segments, electronic packet switching (e.g., Ethernet) is used to maximize the utilization of the networking equipment. Electronic networks are fast reconfigurable: a nanosecond-long packet may be switched from one port to another, and the next nanosecond-long packet may be switched from the same port to another port. Such reconfiguration speed is an enabler for statistical multiplexing, whereby several connections time-share the same physical equipment, such as the transponders and the optical fibers, in order to decrease the amount of deployed equipment. However, with electronic packet switching, all data arriving at a node need to be electronically converted and processed (switched); those operations are both costly and energy consuming when performed at high data rates, such as 100 Gb/s and more per node degree. In addition, the notion of transparency is lost; upgrading a network to a higher data rate requires the upgrade of many or all network elements, while plain OCS only requires the upgrade of the end elements (the transponders)

http://dx.doi.org/10.5772/61990

and not of the ROADM switching elements. For instance, in Figure 1(b), demands A–C and A–D are aggregated into a single data stream at 100 Gb/s sharing the same wavelength due to an electronic switching fabric. Hence, node A requires only two transponders, compared with three transponders in the OCS case. However, the nodes are not equipped with optical switching fabrics and all signals sustain optoelectronic conversions and electronic processing. Demand A–E goes through an electronic switching fabric at node F, requiring an extra transponder at node F compared with the OCS case. Due to statistical multiplexing, a single wavelength is needed between nodes A and B and between nodes B and D.

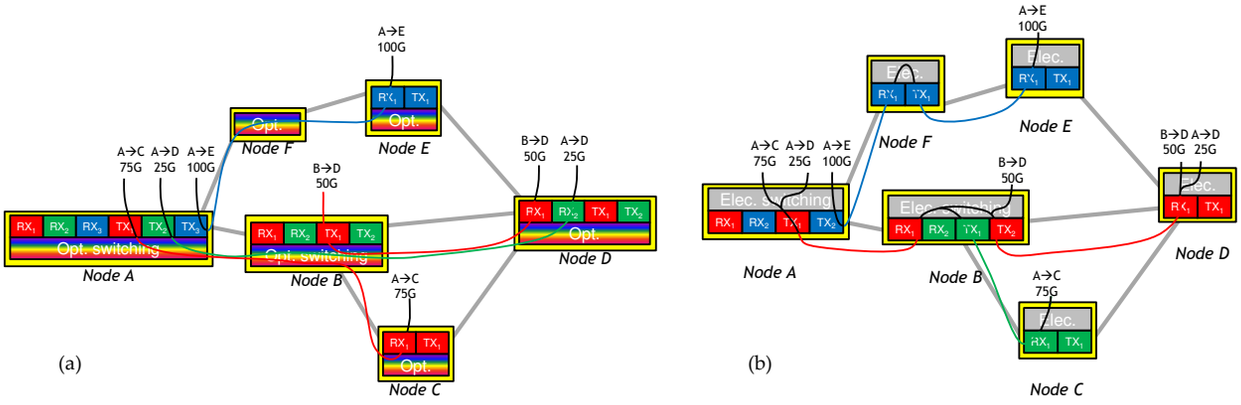

Figure 1. (a) Optical circuit switching (OCS) network. (b) Electronic packet switching (e.g., Ethernet) network.

2.1.3. Optical transport network (OTN)

Recently, the optical transport network (OTN), a transport technology, was introduced to enable sub-wavelength switching in OCS networks. With OTN, the same transponder may be used to send data to several destinations in a TDM fashion, thus enabling statistical multiplexing. At intermediate nodes, similar to standard electronic switching, OTN signals may be regroomed in the electrical domain in order to further optimize the packing of the data on the optical fiber. This requires a dedicated switching fabric, and breaks the optical transparency paradigm for the groomed traffic, similarly to electronic packet switching. In OTN, switching in the optical domain is done with the same slow-reconfigurable switching fabric as that of OCS, making the OTN network less dynamic than the electronic packet-switching network. For instance, in Figure 2, the A–E demand transits transparently through node F, as with OCS. Demands A–C and A–D are groomed together at node A, as in the electronic packet-switching case. As with electronic packet switching, a single wavelength is needed between nodes A and B and between nodes B and D.

2.1.4. Optical packet/slot switching

Optical packet switching (OPS) has been thoroughly investigated in the past two decades. Optical packet switching combines the benefits associated with both fast reconfigurability and dynamics (hence also statistical multiplexing and high-network utilization even under highly

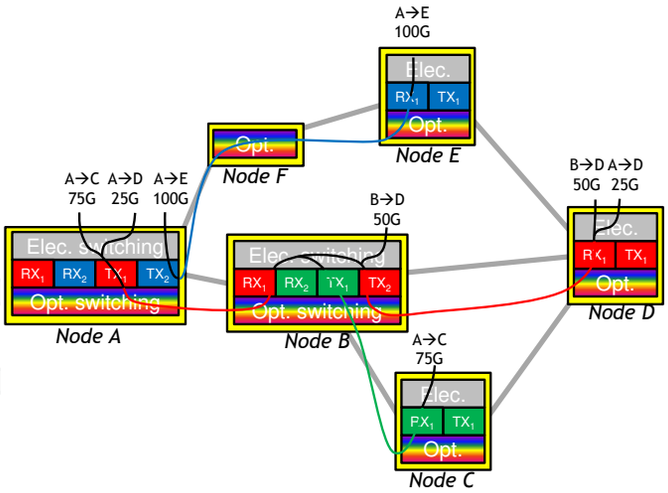

Figure 2. Optical transport network (OTN).

time-varying traffic demands) and optical transparency. With OPS, data are switched at the packet or sub-wavelength granularity directly in the optical domain with no electronic conversion or processing. For instance, in Figure 3(a), all switching is performed in an optical switching fabric at every node, and no electronic switching is required. Demands are groomed, as in the electronic packet switching or the OTN case; however, grooming is performed without optoelectronic conversions; signals may transit transparently through intermediate nodes, as with OCS or OTN. Usually, transmitters or receivers (or both) are fast wavelength tunable, that is, they can switch wavelength between the emission or reception of two consecutive packets. Optical slot switching (OSS) is a version of optical packet switching, where all switched entities are slots of the same duration. While a highly promising technology in terms of network capacity efficiency, energy consumption and flexibility [15], and despite attempts by start-up companies Matisse Networks in the late 2000s and Intune Networks in the early 2010s [16], OPS/OSS has so far not been successfully commercially deployed – essentially due to the lack of the maturity of the target markets (metropolitan and cloud networks) and underlying technical challenges. Indeed, OPS relies on very advanced, disruptive architectures and optical components, which is a very active research topic as of 2016.

Due to their simplicity, optical rings, with nodes of degree 2 only [cf. Figure 3(b)], have been extensively studied in the context of OPS. Many implementations have been proposed for optical packet rings: data and voice integration over dense WDM (DAVID) in 2003 [17], high-performance OPS WDM metro ring network (HOPSMAN) in 2008 [18], optical packet switch and transport (OPST) [19] and packet optical add-drop multiplexers (POADM) [6] in 2009, optical burst transport network (OBTN) [20] in 2011, coherent optical packet ring (COPR) [21] in 2014. Most of these proposals rely on the same component (used under various names), which is denoted here as "packet blocker." This component is able to block selected wavelengths only – the other wavelengths are allowed to cross the component transparently – at the packet granularity. While a wavelength blocker blocks selected wavelengths statically, the packet blocker may block one or several wavelengths on demand during very short periods.

http://dx.doi.org/10.5772/61990

In Figure 3(b), WPB denotes either a wavelength or a packet blocker. The optical packet-switching nodes in the networks cited above typically use a combination of a wavelength or packet blocker, in the drop or in the transit path, or both. Typically, at least one of the blockers is a packet blocker, making it one of the key components of optical packet networks. If the packet blocker is used in an OSS network, it is commonly called "slot blocker." In the transit path, the packet/slot (wavelength) blocker erases the packets/slots that are received or "dropped" by a node and allow insertion or "addition" of new packets/slots (resp., wavelength) on the newly freed wavelength (this is called "wavelength reuse"). When used at the reception side of a node, the packet/slot (wavelength) blocker selects which packets/slots (wavelengths) should be received. In this case, the combination of a packet/slot blocker and of a receiver *de facto* implements a fast-wavelength-tunable packet (or slot) receiver. With coherent systems where the received wavelengths are dictated by the wavelength of a local oscillator, a fast-wavelength-tunable packet/slot receiver can equivalently be built using a fast-wavelength-tunable laser as the local oscillator, removing the need for a packet/slot blocker at reception.

Multi-degree optical packet/slot-switching networks have also been proposed, with less maturity than the simpler degree-2 ring networks, and no commercial implementation or deployment was attempted. Time-domain wavelength interleaved network (TWIN) relies on fast-wavelength-tunable lasers and fiber couplers/splitters, and avoids the utilization of fast blockers, such as the packet blocker [22]. The optical shared memory supercomputer interconnect system (OSMOSIS) project made a different choice and embedded packet blockers as key building blocks, back in 2004 [23]. The interested reader should refer to references [24–25] for other noteworthy implementations of optical packet switches.

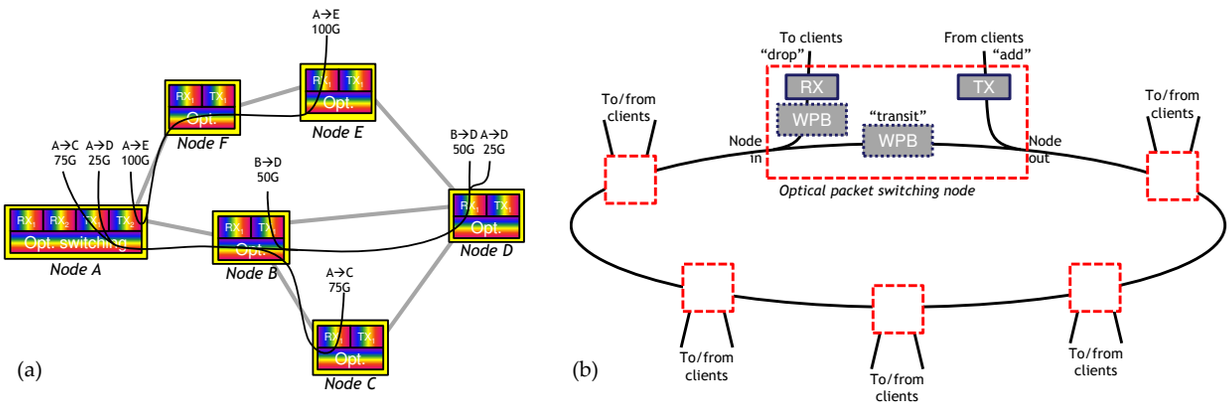

Figure 3. (a) Optical packet-switching (OPS) network. (b) OPS ring network.

2.2. Packet/Slot Blocker Implementation

A typical packet/slot blocker is shown in Figure 4. The wavelength-multiplexed signal is first demultiplexed, then each wavelength goes through a gate, which may block each channel independently based on control signals (not represented in Figure 4), and the wavelengths are

multiplexed before exiting the packet/slot blocker. Due to physical limitations of the various optical components that are used to build optical switches, optical packets must be separated by a "guard interval," during which no data can be transmitted. In order to maximize the utilization of the capacity in the network, packets should be much longer (1–2 orders of magnitude) than the guard interval. With a 10-ns guard interval, packets should be at least 100 ns long, that is, 10000 bits long at 100 Gb/s. This is barely sufficient for standard 1500-byte (12000-bit) IP packets but much longer than the frequent 40-bytes (320 bits) transmission control protocol (TCP) acknowledgments contained in IP packets. Hence, optical packets usually aggregate several client (e.g., Ethernet or IP) packets. Client packet aggregation within optical packets increases network latency, which can be mitigated by reducing the optical packet length or duration. Overall, the packet length or duration should be chosen to be sufficiently large to make the guard interval negligible, yet sufficiently small to mitigate the impact of packet aggregation on network latency. This in turn means that the guard interval should be kept as small as possible, and hence that the optical gates meant to erase optical packets should be as fast as possible. This is quantified by the gate rise time (the time the gate takes to move from the passing to the blocking state) and conversely the fall time, both of which should be minimized.

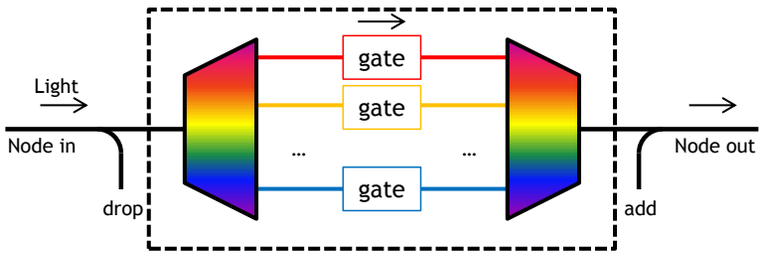

Figure 4. Typical packet/slot blocker consisting of a wavelength demultiplexer, one optical gate per wavelength, and a wavelength multiplexer. The part in the dashed box may be integrated using, for instance, silicon photonics. This "transmitting" implementation requires two connectors.

In addition, optical gates never fully erase light – a small part of the "erased" signal combines with added packets at the output of the packet blocker, causing degradation of the added signal's quality ("crosstalk"), and possibly rendering its decoding impossible. The ratio (in dB) between the power of a packet before crossing a gate and its power after it is erased is called the extinction ratio. In order to minimize signal quality degradations, and thereby to maximize the reach (how many km or how many nodes a packet can cross) of a packet, the gate extinction ratio should be maximized. This is illustrated in Figure 5, where dropped packet (a) on the red wavelength is imperfectly erased by the red gate, causing crosstalk and hence signal quality degradation of packet (b), which is added on the same wavelength.

Figure 4 shows the so-called transmitting implementation of a packet blocker. All blocks within the dashed box may be integrated using one or several technologies, including silicon photonics. However, the cost of such technology is essentially driven by packaging, which largely depends on the number of connectors of the optical chip. The transmitting implementation of the packet blocker shown in Figure 4 requires two connectors. It is possible to substantially

http://dx.doi.org/10.5772/61990

decrease the cost of the packet blocker by removing one connector and replacing it with mirrors, which reflect the light back to the input of the blocker, through the gates and the wavelength demultiplexer, which is then used as a multiplexer. An optical circulator is then used to separate the input and the output ports, as shown in Figure 6(a). This implementation, called a "reflective" packet blocker, additionally improves the extinction ratio as seen by the optical packets since optical packets cross twice the gates, thereby doubling the extinction ratio expressed in dB.

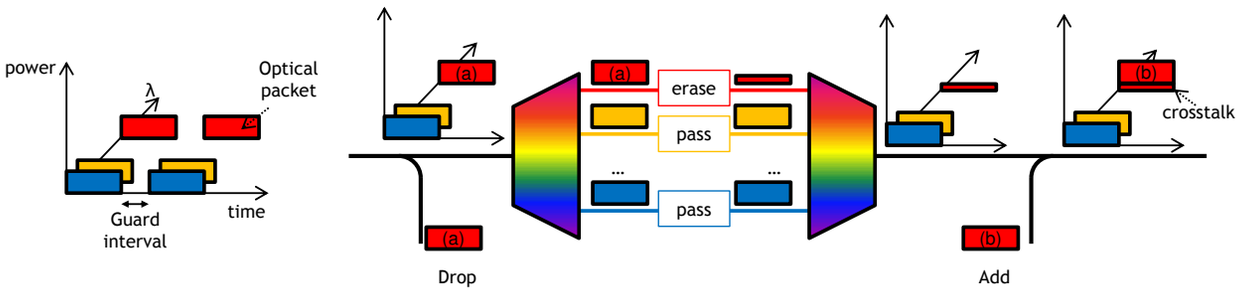

Figure 5. Crosstalk due to imperfect extinction ratio. Dropped packet (a) is imperfectly erased by the red gate; added packet (b) is combined with the leftover power (called "crosstalk") from packet (a), resulting in degraded signal quality for packet (b).

Furthermore, in today's high-capacity networks, signals are encoded on two orthogonal polarizations, transverse-electric (TE) and transverse-magnetic (TM). This doubles the capacity that can be carried by the network at little extra cost. However, some integration platforms are sensitive to signal polarization. In order to ensure compatibility of the packet blocker with dual-polarization signaling, a so-called polarization diversity scheme may be used, as illustrated in Figure 6(b); the wavelength demultiplexer/multiplexer, gates, and mirrors are all duplicated, and each set of components is used by only one polarization, for example, TM at the top of the figure (TE/TM conversion is used in order to ensure that the signal is indeed suitable for the chip) and TE at the bottom of the figure.

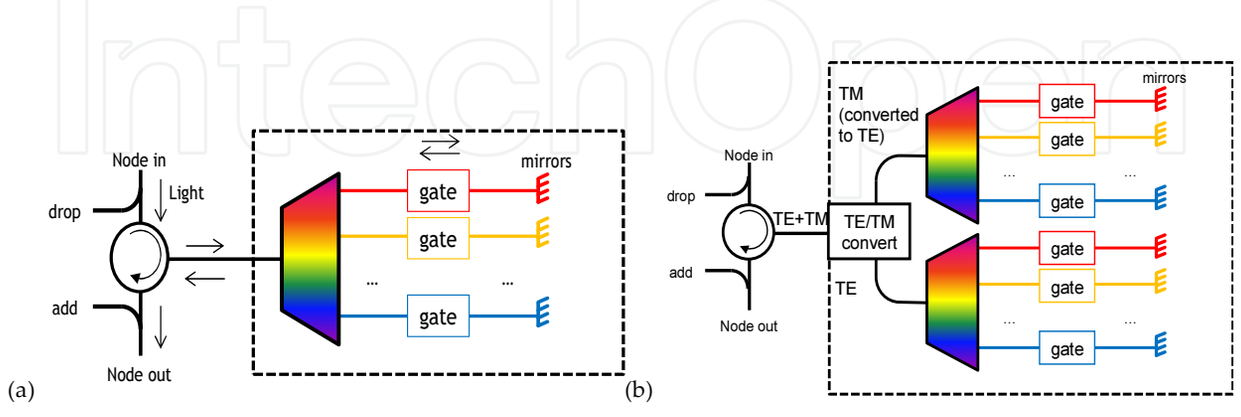

Figure 6. (a) Packet blocker consisting of a circulator, a wavelength demultiplexer, one optical gate, and one mirror per wavelength. (b) Packet blocker with polarization diversity.

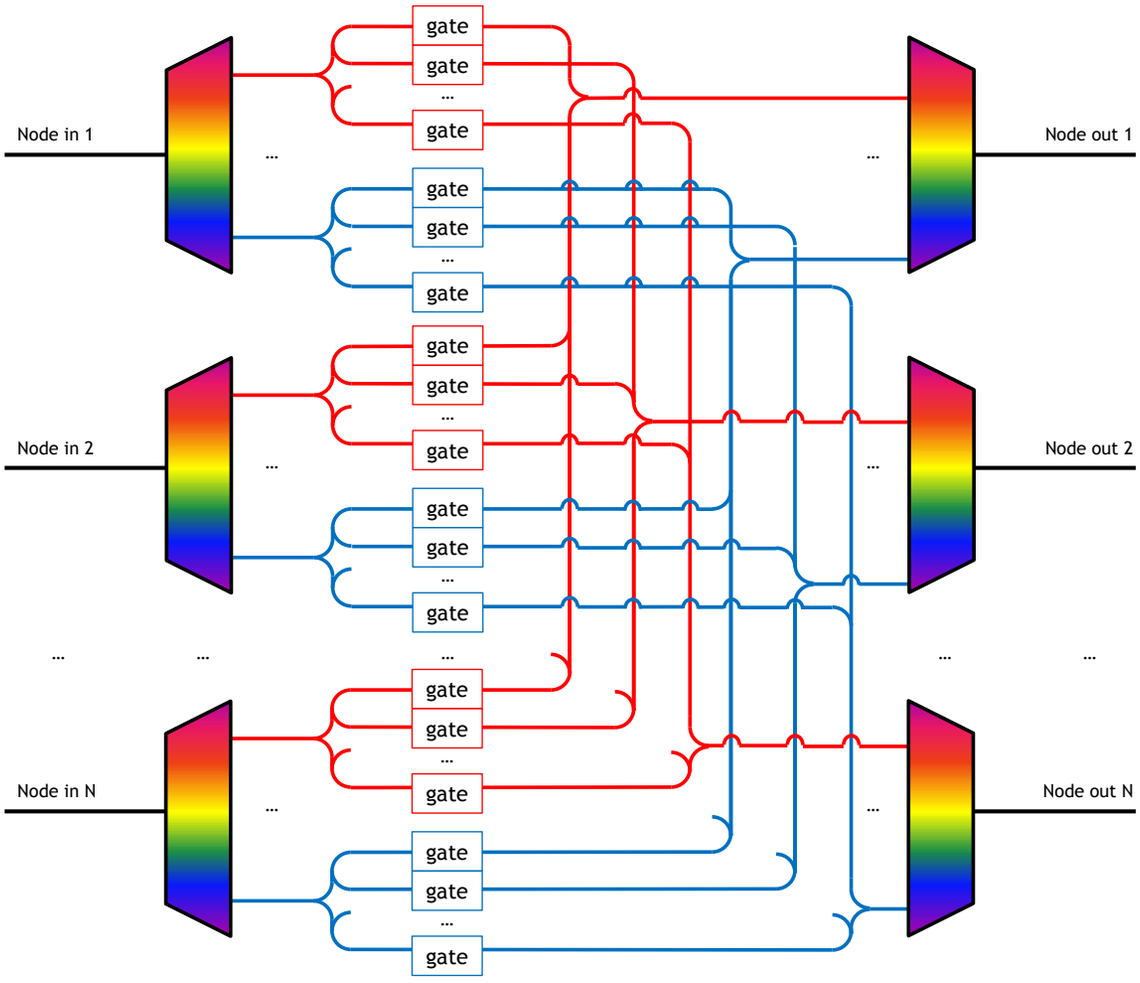

Figure 7. Sample architecture of a multi-degree (*N*) packet blocker based on the broadcast and select technique.

The circulator enables the utilization of the waveguides between the circulator and the mirrors in both directions simultaneously. The part in the dashed box may be integrated using, for instance, silicon photonics. This "reflective" implementation requires only one connector.

It is observed that several of the recently proposed multi-degree optical packet-switching nodes make use of a so-called "broadcast and select" (B&S) architecture [26,28], where an input signal is broadcast (through fiber splitters) to several outputs, each of which is equipped with optical gates to select which input signal will effectively select and forward to the next node. Hence, such architectures generalize packet blockers: in the multi-degree node, gates are used by each output port to select which spatial input – rather than wavelengths as in the slot blocker architecture – should be blocked or passed to the next node. Such spatial switching may further be combined with wavelength switching in more complex node architecture for increased switching capacity. A possible implementation of a multi-degree optical packet-switching fabric, which generalizes the degree-2 packet blocker considered above, is depicted in Figure 7. Not surprisingly, the same technologies that were proposed to implement packet blocker gates can also be used to implement gates in the B&S fabric. Specifically, SOAs are used as described in reference [26] and EAMs are used as described in

http://dx.doi.org/10.5772/61990

[28]. Similarly, the same integration technologies that could theoretically be used to implement a packet blocker can also be used to implement a multi-degree switching fabric, albeit with much increased complexity stemming from the very large number of components to integrate and control, and the waveguide crossings.

3. Semiconductor Optical Amplifier as Optical Gate

SOA is an outstanding candidate for sub-wavelength operations in OPS or OSS. It rapidly switches between blocking and passing states to efficiently suppress or amplify optical signals. To assess the effects that this device brings into optical transmission system, the nature of signal–material interaction inside the SOA should be studied.

3.1. Historical overview

This section presents a historical overview of the network evolution and the semiconductor optical amplifiers. Being aware of the past component evolutions helps to understand the present state of the art and to prepare the future of optical communication. The development of semiconductor materials allowed the fabrication of high-performance devices, such as lasers and optical amplifiers. The development of SOA followed the development of laser diodes. SOAs have a gain medium as in laser devices but with the suppression of the resonance cavity. The stimulated emission concept itself was introduced by A. Einstein in 1917. The feasibility of stimulated emission in semiconductor was demonstrated in 1961 [26,27] and in 1962, the first observation of lasing action in semiconductor materials was done by several research groups [28,29]. The first semiconductor lasers were galliumarsenide (GaAs) homojunction devices operating at low temperature and was called Fabry–Perot laser because of the Fabry–Perot cavity (standard cavity with two mirrors, which are separated by an amplifying medium). Heterostructure design was proposed in 1963 [30] and demonstrated in 1969 [31]. The arrival of heterostructure devices spurred the investigation on SOAs as they were first considered at the beginning as bad lasers. In fact, high-threshold current lasers were attractive to amplify optical beam when they were operated under the lasing regime. Therefore, these first SOAs were called Fabry–Perot SOAs (FP-SOA) and have been deeply investigated [32,33]. In the 1970s, FP-SOAs were not considered seriously as important candidates for optical telecommunication [34,35], which was due to the low gain (operation below threshold current), high-gain ripple, and the instability during the amplification process because of the proximity to the threshold condition. In the 1980s, important achievements on facet reflectivity were realized and a new type of SOAs appeared. In 1982, J. C. Simon reported the first travelling wave SOA (TW-SOA) where the facet reflectivity was around 10^{-3} [36]. The previous drawbacks of FP-SOA were overcome. The threshold current was extremely high and allowed 15 dB of gain; the instability was no longer an issue at relatively high current (~80 mA). Development of high-quality antireflection coating was carried out and the first TW-SOA in indium gallium arsenide phosphide (InGaAsP) system with facet reflectivity of 10^{-5} was realized in 1986 [37]. First SOAs were based on aluminum gallium arsenides (AlGaAs), operating in the 830-nm region [38], then indium phosphide (InP)/InGaAsP SOAs appeared in the late 1980s

[39], centered in the 1.3-μm and 1.5-μm windows. In 1989, polarization-insensitive devices started to become a reality due to symmetrical waveguide structure specially designed for SOAs [40]. Prior to this, SOA structures used laser diode design (asymmetrical waveguide structure) leading to strong polarization-sensitive gain. After the invention of the EDFA, research on SOA (more specifically on TW-SOA) was slowed down for application, such as the in-line amplification, which was the main application at this time. EDFAs were chosen as the preferred solution for in-line amplification in core networks. New applications were investigated in order to take advantage of the important features of SOAs. These devices could be used as elements for all optical switches and optical cross-connects [41,42]. Highly nonlinear phenomena also take place in SOAs and can be used for wavelength conversion and cross-gain modulation [43,44, 48]. Other applications were based on SOA as intensity/phase modulators [45,46], logic gate [47], clock recovery [49, 50], dispersion compensator [51,52], format conversion from no return to zero (NRZ) to return to zero (RZ) [53], etc. The SOA is of smaller size, electrically pumped, and can be potentially less expensive than the EDFA. It can also be integrated with semiconductor lasers, modulators, etc. However, they have not been industrialized as much as EDFAs and this technology has been waiting for market needs. OPS/OSS could be the right application, which needs unique characteristics of SOA.

3.2. Fundamentals of SOA

An SOA is a gain medium based on the stimulated emission. The purpose of optical amplifiers is to increase the power of the incoming signal. The input signal or light is amplified along the amplification zone. The amplification takes place in the active zone only if an external current supply is provided (considering electrically pumped device). The optical gain is associated with the stimulated emission process, which requires the recombination of electron–hole pairs. Without electrical injection, the SOA would absorb the incoming photons. RSOA is a particular scheme of SOA, which stands for reflective SOA. A mirror is inserted at the output of the device in order to reflect back light into the amplification zone. Therefore, the input and output of the device are at the same facet and the device can be more compact because of the forward and backward amplifications. SOA devices can operate in these three configurations:

1. TW-SOA using ultralow reflective end facets
2. FP-SOA where the reflections at the end facets are significant
3. RSOA where one facet is highly reflective and the other one has low reflectivity

Facet reflectivity is one of the key parameters in SOAs to form TW devices, optical cavities, or to redirect light to other directions. SOA components need a careful control on reflection from its end mirrors. Losses due to the facet reflectivity are a key parameter for mode selection. Depending on what is needed, they can be either minimized or maximized.

Gain in a semiconductor material results from current injection into the PIN structure. The relationship between the current / and the carrier density could be given by the rate equation where the carrier density is nearly uniform along the transverse dimension and neglect carrier diffusion as in reference [54]:

http://dx.doi.org/10.5772/61990

$$\frac{\partial n}{\partial t} = \frac{\mathrm{I}}{\mathrm{q.V}} - \frac{\mathrm{n}}{\tau_c} - \frac{\mathrm{g(n)}}{h\nu}\left|\mathrm{A}\right|^2 \tag{1}$$

where n is the carrier density, I is the injection current, q is the electron charge, V is the active volume, τ_c is the spontaneous carrier lifetime, and $h\nu$ is the photon energy.

The optical gain dependence on the photon energy and the carrier density is quite complex. However, it can be approximated using simple expressions:

$$g_m(\lambda, n) = a \times \Delta n - a_2\left(\lambda - \lambda_p\right)^2 \tag{2}$$

where $\lambda_p = \lambda_0 - b_2\Delta n$, $a = \frac{\partial g}{\partial n}$ is the differential gain, $\Delta n = n - n_0$ is the carrier density variation, where n_0 is the carrier density at transparency, a_2 is a constant related to the spectral width of the gain spectrum, and λ_0 is the operating wavelength.

The use of the separate heterostructure is important in order to optimize the electronic and the optical confinement. The optical field overlaps not only the active medium but also the parts around it. The amplification takes place in the active region. Only a part of the optical field, confined in this region, takes part in the stimulated emission; therefore, the optical gain (g) in equation (2) is not just equal to the material gain. The waveguide modal attenuation coefficient α_{in}, which characterizes the internal losses and the confinement factor as Γ, can be defined. These losses decrease the overall modal gain, and the net mode gain can be defined by:

$$g_{net} = \Gamma . g_m - \alpha_{in} \tag{3}$$

The internal losses can be decomposed into two different losses (α_a, α_c). The modal loss in the active region is defined by $\Gamma\alpha_a$ and the modal loss in the cladding region is defined by $(1\text{-}\Gamma)\alpha_c$. Thus, the total internal modal loss can be written as:

$$\alpha_{in} = \Gamma\alpha_a + (1 - \Gamma)\alpha_c \tag{4}$$

It is common practice to model gain saturation by equation (5) [54]. However, this equation ignores the distributed loss, so a new phenomenological parameter (ε) is introduced to fit the gain versus power experimental curves:

$$\frac{\ln G_0 - \ln G(P)}{G(P) - 1} = \left(\frac{P}{P_{sat}}\right)^{1+\varepsilon} \tag{5}$$

where G_0 is the SOA small signal gain, P is the input optical power, and P_{sat} is the SOA saturation power.

In Figure 8(a), the best match for ε is $\varepsilon = 0.26$ in the least-mean square sense, as evidenced by the theoretical curve of Figure 8(a). The small signal gain is optical gain produced when SOA is operating with low-input optical signal power. Modern commercially available SOAs demonstrate fiber-to-fiber gain of 20 dB over the C-band with a gain peak centered around 1550 nm. P_{sat} is an output optical power that manifests gain decrease (saturation) by 3 dB. Depending on technology and application field, one may currently find SOAs with 6–16 dBm of saturation power. Another important parameter is the noise figure (NF), which is the ratio between signal-to-noise ratio (SNR) before and after the SOA and it is defined as:

$$\mathrm{NF} = \frac{\mathrm{SNR}_{\mathrm{in}}}{\mathrm{SNR}_{\mathrm{out}}} \tag{6}$$

where $\mathrm{SNR}_{\mathrm{in}}$ is the signal-to-noise ratio at the input of the SOA and $\mathrm{SNR}_{\mathrm{out}}$ is the signal-to-noise ratio at the output of the SOA. Typical noise figures of commercial SOAs are in the range from 8 dB to 11 dB. The optical SNR (OSNR) degradation after an optical amplifier is calculated based on the formula:

$$\frac{1}{\mathrm{OSNR}_{\mathrm{out}}} = \frac{1}{\mathrm{OSNR}_{\mathrm{in}}} + \frac{\mathrm{NF} \times h\nu \times B_{\mathrm{ref}}}{P_{\mathrm{in}}} \tag{7}$$

where $\mathrm{OSNR}_{\mathrm{in}}$ is the input OSNR, NF is the noise factor, P_{in} is the input optical power, and B_{ref} is the reference bandwidth (0.1 nm).

The spontaneous emission is created inside the active zone producing extra noise during the amplification. The spatial distribution of the carrier density is then strongly affected by this process. The spontaneous emission is produced all along (every z) the device. A part of the emitted photons are guided and amplified. They form the amplified spontaneous emission (ASE). The main noise contribution is attributed to the ASE noise [56] and OSNR degradation takes place due to the ASE noise. A given OSNR is needed to ensure specific BER values. Therefore, there is only a finite number of SOA (i.e., a finite number of spans), which could be cascaded to ensure a given BER. The output OSNR after traversing one SOA and depending on the input optical power is presented in Figure 8(b). According to equation (7), the output OSNR degrades at low input power (due to higher noise accumulation); therefore, BER increases. In order to mitigate its impact, higher input power needs to be injected into the SOA. However, as ASE noise limits minimal input optical power, the nonlinear behavior of SOA limits the maximum input optical power. Therefore, BER increases at high input power even if the OSNR is not degraded.

http://dx.doi.org/10.5772/61990

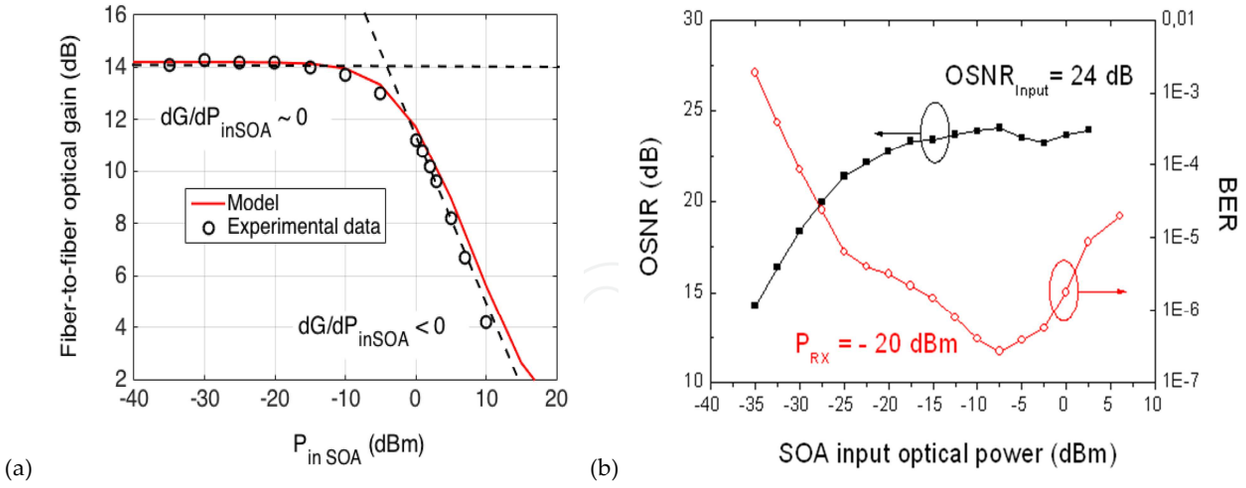

Figure 8. (a) Measured and modeled SOA optical gain. (b) BER for a 10 Gbit/s OOK-NRZ signal and OSNR measurements depending on the SOA input optical power.

We can approximate that SOA parameters responsible for nonlinear effects are spontaneous carrier lifetime (τ_c) and line-width enhancement factor (α). As SOA has the same active medium as semiconductor lasers, carrier lifetime is in the range of 200–700 ps. The carrier lifetime is inversely proportional to the recombination rate. The photon density from the amplified signal and the spontaneous emission affects the carrier density. Since photon density is not homogeneous along the SOA, carrier density also depends on the position. This spatial hole burning (SHB) is also present in many lasers, but it results from the coupling between carriers and a single photon population. These saturation effects strongly influence the static and dynamic performances of SOAs [57,58]. A multi-section model could be considered in order to take into account such spatial distribution; more details on simulations along the SOA length can be found in reference [59] and in the following section. In this section, we will consider the carrier lifetime as constant for sake of simplicity. Factor α also known as Henry factor (after Charles Henry who explained the line-width enhancement phenomenon in reference [60]) is responsible for line-width broadening after the SOA and has values within the range from 4 to 7.

The signal power and the phase are found to satisfy [54]:

$$\frac{\partial P}{\partial z} = g(z,\ \tau)P$$

$$\frac{\partial \Phi}{\partial z} = \alpha_{\mathrm{H}} \frac{g(z,\ \tau)}{2} \tag{8}$$

It can be easily demonstrated by combining both equations that:

$$\alpha_{\mathrm{H}} = 2P\frac{\partial \Phi}{\partial P} \tag{9}$$

where $\frac{\partial \Phi}{\partial P}$ is the variation of the phase over the variation of the optical power.

It has been shown that SOAs can be used in order to control the chirp of an input optical pulse [61]. The chirp parameter α_H is defined as in equation (9). Assuming the Δn is homogeneous along the SOA, the gain variation (from the single-pass gain expression) can be written as:

$$G = e^{\Gamma a \Delta n L} \tag{10}$$

So the gain variation in dB can be written as:

$$\Delta G_{\mathrm{dB}} = \Gamma a \Delta n L \cdot 10 \log_{10}(e) \tag{11}$$

And the phase variation as:

$$\Delta \Phi = -\frac{2\pi}{\lambda} \cdot \Delta n_{\mathrm{ref}} L = \frac{\alpha'}{2} \Gamma a \Delta n L \tag{12}$$

where λ, n_{ref}, and L are wavelength, refractive index, and SOA length, respectively. α' is the line-width enhancement factor of the semiconductor material, which is defined as:

$$\alpha' = -\frac{4\pi}{\lambda \Gamma a}\left(\frac{\partial n_{\mathrm{ref}}}{\partial n}\right) \tag{13}$$

The alpha factor depends on the gain variation under modulated input optical power. It can be demonstrated as in reference [62]:

$$\alpha_H = \alpha' \frac{dG / dP_{\mathrm{in\ SOA}}}{1 + dG / dP_{\mathrm{in\ SOA}}} \tag{14}$$

where P_{in} is the SOA input optical power.

When the optical input power is low enough, equation (14) gives α_H=0 because the carrier density remains unchanged compared to the value at the equilibrium (Δn = 0) and $dG/dP_{\mathrm{in}} \sim 0$. No gain variation is observed as represented in Figure 8(a), so no degradation of the optical signal should be observed even with high line-width enhancement factor (α'). However, as the optical input power increases, carrier depletion occurs in SOA ($\Delta n < 0$) and induces gain saturation ($\mathrm{d}G/\mathrm{d}P_{\mathrm{in}} < 0$). Since $\alpha' > 0$ in gain medium, such as in SOA, the chirp parameter is negative ($\alpha_H < 0$) for the gain-saturated SOA. The frequency components of the

http://dx.doi.org/10.5772/61990

leading edge of the pulse are red-shifted and trailing edge blue-shifted when the chirp is negative ($\alpha_H<0$) as explained in reference [61]. Therefore, a trade-off arises between nonlinear distortions (at high input power) and noise (at low input power) and an optimum input power can be defined. The impact of the line-width enhancement factor on the signal integrity (mainly adding phase noise) is studied in Section 3.3.3.

3.3. SOA Model and Simulation

3.3.1. Analytical model for OOK-NRZ signal

In this section, we propose an analytical model to predict the impact of SOA devices on an NRZ optical signal [63]. In the linear regime (before gain saturation), the NF is used to predict the OSNR degradation as explained previously. However, when the input optical power becomes higher, such formula does not apply anymore as the main degradation of the signal comes from the nonlinear behavior of the SOA. To assess the nonlinear impairments due to the SOAs, we study the evolution of the OSNR penalty for a given target BER, as a function of SOA input power and of the number of cascaded SOAs. Here, the OSNR penalty is the difference between the required OSNRs (in dB) to ensure the target BER (here, $BER_t = 10^{-3}$) after traversing SOAs and in back to back. We assume here that the distortions of the signal can be described by the extinction ratio r (amplitude modulation only), defined as $r = P_1/P_0$, where P_1 and P_0 are the average powers of marks and spaces, respectively. The relationship between OSNR and BER is given as in reference [64]:

$$\mathrm{BER} = \frac{1}{2}\mathrm{erfc}\left(\frac{\mathrm{Q}}{\sqrt{2}}\right) \tag{15}$$

$\mathrm{Q} = \frac{\sqrt{\mathrm{r}}-1}{\sqrt{\mathrm{r}}+1}\sqrt{\frac{\mathrm{OSNR_{ref}} \times \mathrm{B_{ref}}}{\mathrm{B_e}}}$, where erfc(.) is the complementary error function, B_{ref} is the optical bandwidth for which the measured OSNR (12.5 GHz in this work) is expressed, and B_e is the receiver electrical bandwidth. Thus, for a given value of r, the OSNR penalty $Pen(r)$ (in dB scale) can be easily derived [63]:

$$Pen(r) = 20\log\left(\frac{\sqrt{r}+1}{\sqrt{r}-1} \times \frac{\sqrt{r_0}-1}{\sqrt{r_0}+1}\right) \tag{16}$$

where r_0 is the extinction ratio in back to back.

We now explain how the saturation of the SOA gain can impact r when an OOK-NRZ signal goes through. At low-input power levels, below −20 dBm, in the linear regime, the gain of the SOA is independent of the input power, and we expect no impact on the extinction ratio of an incoming signal. At high power levels, the SOA turns nonlinear, and the SOA gain saturates and decreases [Figure 8(a)]. Thus, we expect a decrease of the extinction ratio of an incoming

signal at SOA output. Optical gain saturation could be modeled as described in the previous section. Let us suppose we have N identical cascaded SOAs, and that the input optical power into each SOA is fixed to P_{in} employing variable optical attenuators at the SOA inputs. The extinction ratio at the output of the k^{th} SOA, where $k = 1, \ldots, N$, is denoted by r_k, and the average optical powers of "1" and "0" at the input of the k^{th} SOA are denoted by $P_1^{(k)}$ and $P_0^{(k)}$, respectively. For $k = 1, \ldots, N$, it can be written as:

$$P_1^{(k)} = \frac{2r_{k-1}P_{\text{in}}}{1+r_{k-1}} \quad \text{and} \; P_0^{(k)} = \frac{2P_{\text{in}}}{1+r_{k-1}} \; \text{and} \; r_k = \frac{P_1^{(k)}G(P_1^{(k)})}{P_0^{(k)}G(P_0^{(k)})} \tag{17}$$

With such an analytic model, we can iteratively estimate the degradation of the extinction ratio after the cascade of SOAs and deduce the OSNR penalty, regardless of the input power or the number of cascaded SOAs. The nonlinearity accumulation could then be extracted for a large number of cascaded SOA as explained in Section 4. In order to analyze the impact of SOA device on high-order modulation format, a more complex model is needed as described in the following section.

3.3.2. SOA multi-segment model for high-order modulation format

Coherent optical transmission systems may be deployed in metropolitan and data center networks in the near future as detailed in Section 1. These systems operate with QPSK and QAM signals that use both amplitude and phase of the optical signal to transmit information. To assess the impact of the SOA cascade on such signals, we need to use models that can simulate the evolution of carrier density along the active zone of the SOA with high precision. The computation complexity of the model should be taken into account when the task is to analyze a large cascade of the SOAs in optical transmission line via numerical simulation. As a trade-off between precision and complexity, we find that a multi-segment SOA model is a suitable solution to assess the impact of the SOA on optical signals in coherent transmission systems. Such model from reference [65] demonstrates sufficient accuracy and enables study of cascades of numerous SOAs in a reasonable time. As pointed out in reference [66], one may transform this model in two ways. First, further simplification with small perturbation approach will provide a low-complexity SOA simulator for small signal cases. Second, adding equations of SHB and carrier heating (CH) augments the complexity but provides a simulator sensitive to these ultrafast phenomena. However, characteristic time of gain recovery from SHB and CH is less than 10 ps as presented in reference [67], and thus they should have no impact on optical signal below 100 GHz frequencies (our range of study). To make the model suitable for static and dynamic analysis, some assumptions have been made and simplifications have been introduced. The material gain is assumed to vary linearly with the carrier density but with no wavelength dependence as described in reference [68]. The total device length is divided into smaller sections, where the carrier density is assumed to remain constant, in order to simulate the carrier density variation. More details are presented in reference [59]. Scheme of the proposed SOA model is presented in Figure 9. We used a model with ten

http://dx.doi.org/10.5772/61990

segments in our simulations. Each segment consists of three stages: amplification, ASE addition, and internal loss section. The premise to segmentation and stage separation solution was formed using the technique proposed in reference [54]. To obtain a relatively simple equation for SOA gain stage [as equation(10)], spontaneous emission processes as well as internal loss were neglected. Therefore, second (ASE) and third (loss) stages were added for completeness of the model. Moreover, to consider signal–noise interactions and loss influence on traversing signal, one should use several segments such that ASE noise and loss from previous segments will affect signal evolution in the subsequent ones.

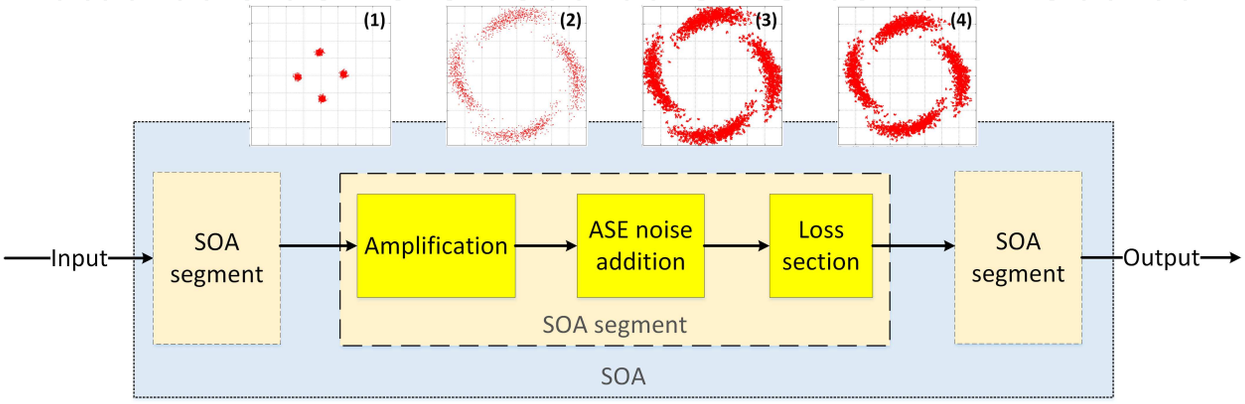

Figure 9. Scheme of SOA segmented model ([2]) with QPSK constellation evolution after each stage: constellation at the segment input (1), after amplification stage (2), after ASE addition (3), and after loss section (4).

According to reference [54], equation. (1) could be written such that the first stage of each SOA segment is an amplification stage where we calculate SOA gain due to stimulated emission from:

$$\frac{\partial h(t)}{\partial t} = \frac{h_0 - h(t)}{\tau_c} - \left(e^{h(t)} - 1\right)\frac{P_{in}(t)}{P_{sat}\tau_c} \tag{18}$$

with h being the SOA gain integrated along the segment's length, h_0 small-signal gain per segment, saturation power P_{sat}, and incident optical power P_{in}. We use Runge-Kutta method (RK4) to solve this equation for signal symbol by symbol. After we obtain $h(t)$, we are ready to calculate output optical field $A_{out,amp}(t)$ after the amplification stage:

$$A_{out,amp}(t) = A_{in}(t)e^{\frac{h(t)}{2}(1-j\alpha_H)} \tag{19}$$

where α_H is the alpha factor of the SOA as described by equation (14).

The second stage is ASE addition. To calculate the ASE noise, one would also use the obtained gain values from equation (18):

$$A_{\mathrm{ASE}}(t)=\sqrt{\mathrm{NF}\left(e^{h(t)}-1\right)h\nu B_0}\left(n_I(t)+jn_{\mathrm{Q}}(t)\right) \tag{20}$$

with NF denoting noise figure, $h\nu$ denoting signal photon energy, B_0 denoting noise integration bandwidth at the receiver, $n_I(t)$ and $n_Q(t)$ denoting independent Gaussian processes for ASE randomness simulation.

The third stage is dedicated to loss simulation. Usually, internal SOA loss is considered constant and optical field after one SOA segment may be written as follows:

$$A_{\mathrm{out,seg}}(t)=\left(A_{\mathrm{out,amp}}(t)+A_{\mathrm{ASE}}(t)\right)e^{\alpha_{\mathrm{int}}} \tag{21}$$

where α_{int} is SOA internal loss per segment.

3.3.3. SOA parameters impact on signal quality

To evaluate the impact of SOA parameters on passing optical signal, we have simulated SOAs with different parameters and calculated relative deviation. We used 2^{15}-1 pseudorandom bit sequences (PRBS) modulated at 10.7 Gbaud in NRZ QPSK signal with initial OSNR of 40 dB at two input optical powers: −30 dBm for the small-signal regime and +5 dBm under gain saturation regime. Our SOA parameters were as follows: 14.2 dB small-signal gain, 5 dBm saturation power, noise figure of 8 dB, line-width enhancement factor of 5, and carrier lifetime of 400 ps. Then, we varied one of these parameters and observed the output optical signal evolution. We calculated relative amplitude deviation $\Delta A/A_{\mathrm{ideal}}$ (RAD) and relative phase deviation $\Delta\varphi/\varphi_{\mathrm{ideal}}$ (RPD) based on received signal constellations as detailed in Figure 10. Our metrics are normalized in such way that RAD and RPD should be equal in the case of Gaussian white noise around the symbols.

Changing small-signal gain has little influence on generated noise while in unsaturated regime, as can be seen in Figure 11(a). Here, augmenting gain means augmenting both amplitude and phase noise. During saturation, increase in gain translates into more abrupt saturation and, therefore, larger amplitude fluctuations. Amplitude noise couples with phase noise through alpha factor; therefore, we observe that both noises grow. Saturation power determines where saturation begins to manifest. While saturation power grows, the SOA becomes a more linear amplifier (keeping the input optical signal power constant). That means less gain fluctuations and less noise as well, as demonstrated in Figure 11(b). Noise figure is proportional to the ASE noise generated within the SOA. In small-signal regime, the ASE noise is prevailing and NF increase manifests equivalently in both amplitude and phase noise, as presented in Figure 12(a). Remarkably while in saturation, nonlinear effects exceed ASE impact to such an extent that we observe no influence of the NF. Carrier lifetime is a characteristic of how fast gain reacts to input power changes. While SOA works with small input powers, its gain does not vary and carrier lifetime has no impact on amplitude and phase noises as shown in Figure

http://dx.doi.org/10.5772/61990

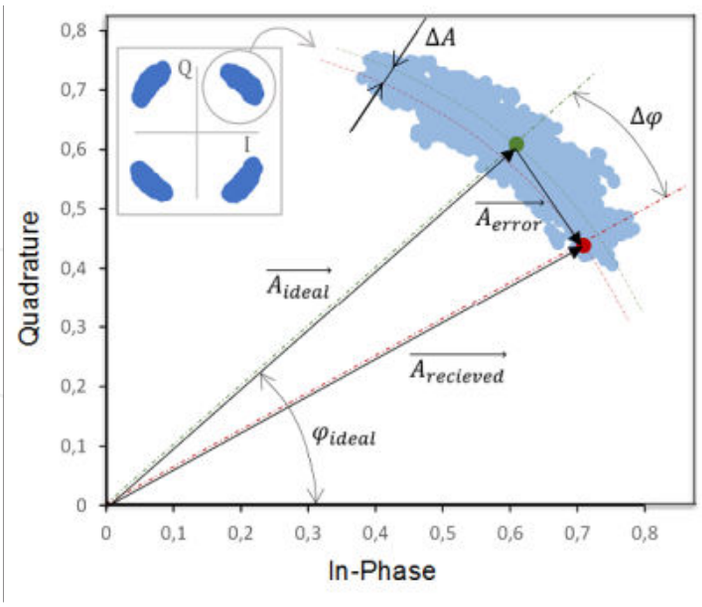

Figure 10. QPSK constellation symbol upon reception. Ideal transmitted symbol is shown with $\overrightarrow{A_{ideal}}$ and illustrative received symbol – with $\overrightarrow{A_{received}}$. Amplitude error ΔA, phase error Δφ and error vector $\overrightarrow{A_{error}}$ are demonstrated.

12(b). However, when carrier lifetime decreases, the SOA's gain dynamics becomes fast enough to follow shorter signal power changes producing amplitude and phase noise, the so-called bit-patterning effect. We observe the resonance when the parameter becomes equal to the inverse of signal's symbol rate (1/10.7 GHz = 93 ps). Further decrease in carrier lifetime accelerates gain recovery, which diminishes SOA contribution to optical noise.

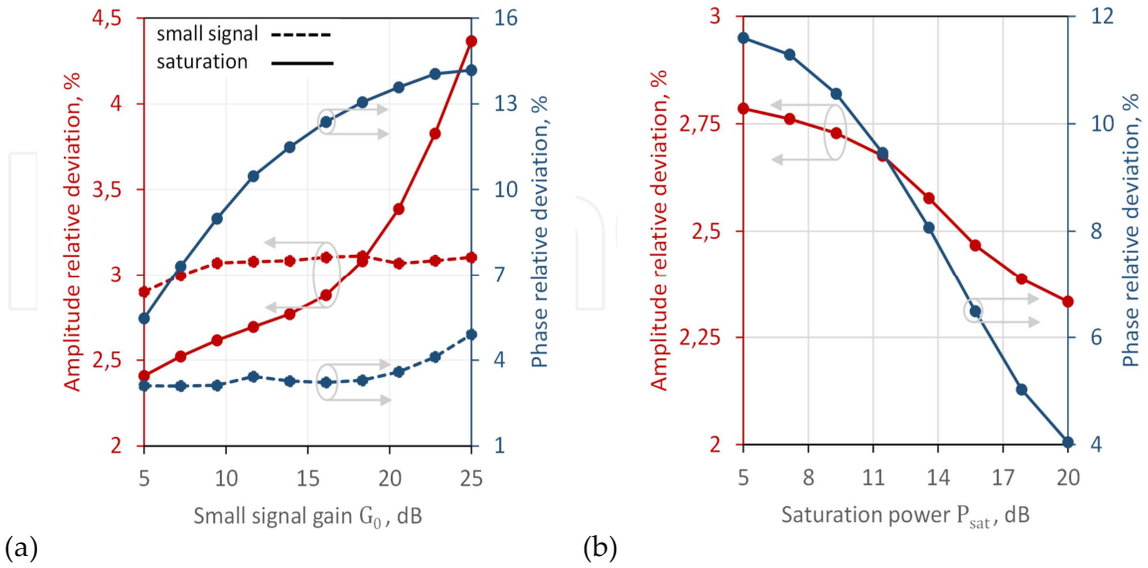

Figure 11. Relative amplitude (in red) and phase errors (in blue) for different small-signal gains (a) and saturation powers (b) of the SOA. Dashed line corresponds to small-signal mode and solid line corresponds to gain saturation mode.

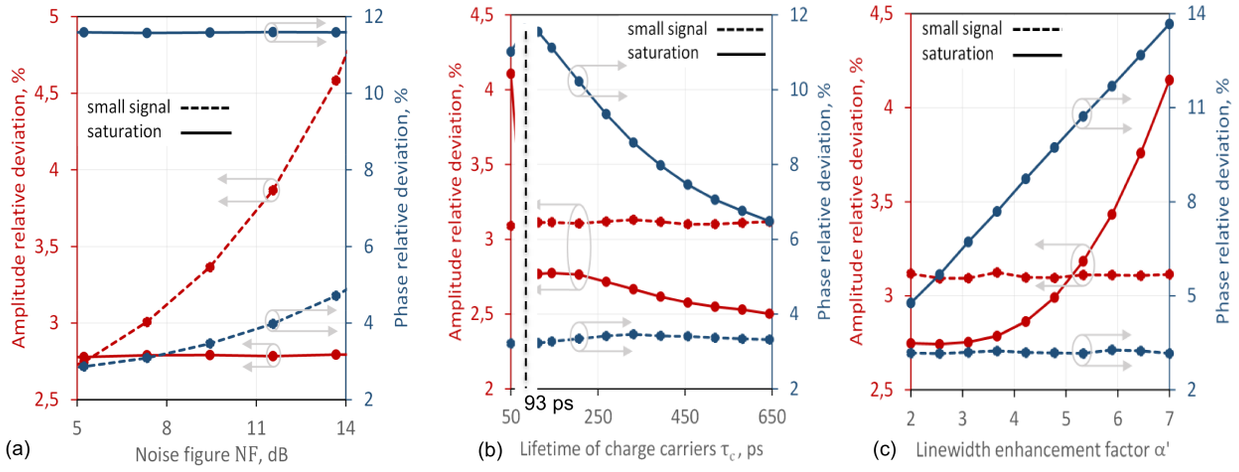

Figure 12. Relative amplitude (in red) and phase errors (in blue) for different noise figures (a), for different charge carriers lifetimes (b), and line-width enhancement factors of the SOA (c). Dashed line corresponds to small-signal mode and solid line corresponds to gain saturation mode.

Factor α' translates the input power fluctuation into gain changes and phase changes. No gain change in small-signal regime is observed for any input optical power [as predicted in Figure 8(a)]; therefore, α' does not impact the quality of the signal as demonstrated in Figure 12(c). In the saturation regime, α' determines the nonlinear phase noise of the SOA and as α' grows, phase noise increases.

4. Cascade of SOA

In optical packet-switched network, the optical packet could travel across a large number of nodes. Therefore, the technology used for the logic gate strongly impacts the system performance and could limit the operating power range. Thus, an estimate of the OSNR penalties is needed to design a complete system, as described in the next section.

4.1. Design Rules for SOA-based Optical Network

4.1.1. Direct detection technology: on–off keying

An analytical model was proposed in Section 3.3.1. Such model predicts the OSNR penalty due to the extinction ratio degradation as the signal goes through a series of SOAs. Such degradation is defined by the optical gain profile as presented in Figure 8(a) and translated to a BER degradation, as observed in Figure 8(b). In Figure 13(a), the modeled OSNR penalty is plotted against the product between the SOA average input power $P_{\text{in SOA}}$ and the number N of cascaded SOAs (in dB scale, i.e., $10\log_{10}[N \times P_{\text{inSOA}}(\text{dBm})]$), versus input powers between [−30 dBm; +7 dBm] and up to 50 cascaded SOAs. The SOA parameters are the same as detailed in reference [63]. We observe that all points gather almost on a single curve. Hence, it is tempting

http://dx.doi.org/10.5772/61990

to approximate the penalty as a function of the product $N \times P_{\text{inSOA}}$. Such a behavior is similar to that observed in the cascade of fiber spans in dispersion-managed systems under the influence of Kerr nonlinear effect [55]. The OSNR penalty was shown to scale as a function of the sum of the input powers into each line fiber span, (or more accurately as a function of the nonlinear cumulated phase). By analogy with reference [64], the product $N \times P_{\text{inSOA}}$ will here be referred to as the integrated power (IP), which could be generally defined as:

$$IP = \sum_{SOA\ k} P_{in\ SOA}^{(k)} = P_{in\ SOA} \times N \tag{22}$$

In direct detection systems with chromatic dispersion (CD) compensation, a maximum of 1.5 dB OSNR penalty is usually accepted for fiber-induced nonlinear penalties [64]. According to Figure 13(a), the range of possible values of integrated power leading to such threshold penalty does not exceed 1.6 dB with N ranging from 1 to 50 sections, which is reasonably accurate. By analogy with cascades of fiber spans, we also define the nonlinear threshold (NLT) as the minimum value of integrated power leading to the threshold penalty. In order to derive general design rules, the NLT (for 1.5 dB of OSNR penalty) has been modeled depending on the optical gain, the saturation power as represented in Figure 13(b). Therefore, it is possible to find out the NLT as a function of the SOA design or/and the operating condition. Low optical gain and high saturation power are mandatory in order to optimize such NLT. In Section 4.2.1, after checking that the $N \times P_{\text{inSOA}}$ behavior is also observed experimentally from a more limited number of cascaded SOAs (up to 4), we will experimentally characterize the NLTs of the (R)SOA devices under study and use them to derive the maximum acceptable number of cascaded SOAs.

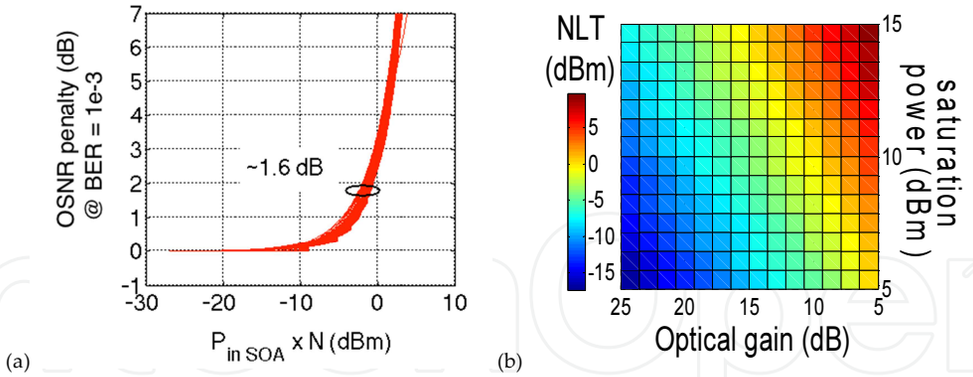

Figure 13. (a) Modeled OSNR penalty for SOA devices depending on $N \times P_{\text{in SOA}}$ for 10 Gbit/s NRZ signal and (b) NLT dependence on SOA parameters (G, P_{sat})

4.1.2. Coherent technology: advanced modulation formats

We simulate an optical fiber line including SOA (based on the 10-section model presented in Section 3.3.2) and optical fiber with a 28-Gbaud RZ optical signal path through a cascade of SOAs. We use root-raised cosine filter with 0.1 roll-off for pulse shaping a payload of 2^{15}–1 symbols. Compared to experimental evaluation, the simulated input optical signal has less

optical power fluctuation; therefore, we chose an RZ signal in order to emphasize the nonlinear impact of SOA. We implement the multi-section model described in Section 3.3.2 with 10 sections. All SOA model parameters are detailed in reference [69]. Single-channel and single-polarization QPSK, 8-QAM, and 16-QAM optical signals are launched into a cascade of SOAs. For each simulation, we vary the input power of the SOAs. We plot OSNR penalty as a function of the IP. In the case of nonlinear noise occurring in fiber networks without inline CD compensation, the threshold OSNR penalty equals 1.76 dB providing the best transmission quality [70]. We use the same penalty to assess the NLT after the cascade of SOAs. We investigate the convergence of OSNR penalty curves depending on the IP for different modulation formats in Figure 14(a) as described for OOK signals. The modeled OSNR penalty is plotted against the IP (in dB scale).

A maximum IP spread of 2.6 dB and 1.5 dB are obtained for QPSK and M-QAM signals, respectively (spread of 1.6 dB was obtained with OOK signals) [69].

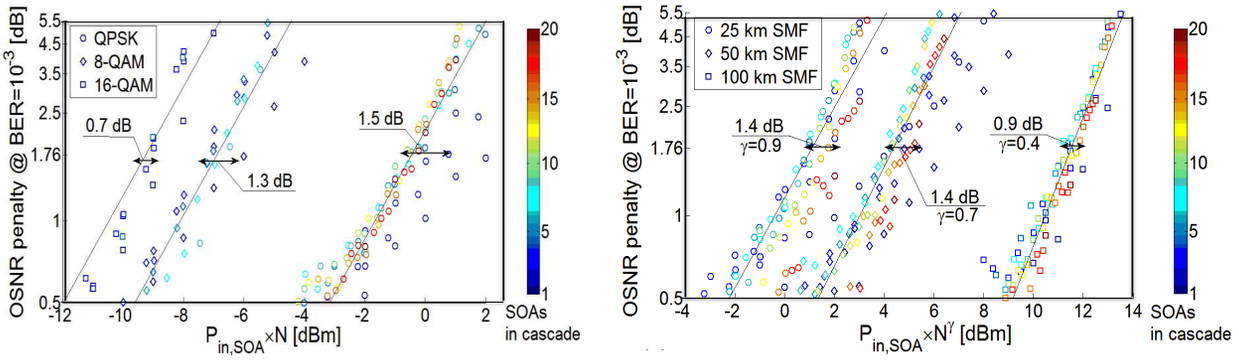

Figure 14. OSNR penalties (a) for a cascade of 20 SOAs with QPSK, 8-QAM, and 16-QAM signal and (b) for a cascade of 20 SOAs with 25 km, 50 km, and 100 km of single-mode fiber (SMF) spans.

We simulate different types of spans including 25 km, 50 km, and 100 km of SMF and one SOA with a 100-G QPSK signal in Figure 14(b). We have introduced a new phenomenological parameter γ in order to take in account the changing character of the nonlinear accumulation when using extra optical fibers. Therefore, a more general law $IP_g = P_{in} \times N^{\gamma}$ is introduced and presented in Figure 14(b).

A compromise between cumulated nonlinear distortions and ASE noise need to be taken in account when optimizing the number of cascaded devices. The evolution range of SOA input powers with respect to the maximum number of cascaded nodes is presented in Figure 15. This model used the nonlinear threshold of the Figure 14 to set the maximum input power into the SOAs. The OSNR degradation is calculated based on the NF of the SOA. An OSNR margin of 3 dB (at BER = 10^{-3}) with respect to back to back is assumed for aging and implementation penalties as well as 1.5 dB of penalty coming from the nonlinear behavior of the SOA (worst-case estimation). Therefore, the maximum number of cascaded devices for a given input optical power is reached when the targeted OSNR is obtained. The OSNR is expected to remain above the OSNR limit and the integrated power needs to remain below the NLT. The largest count of cascadable devices is obtained at the optimal trade-off between nonlinear distortions and ASE noise. ASE noise accumulates from one device to the next. In order to mitigate its impact,

http://dx.doi.org/10.5772/61990

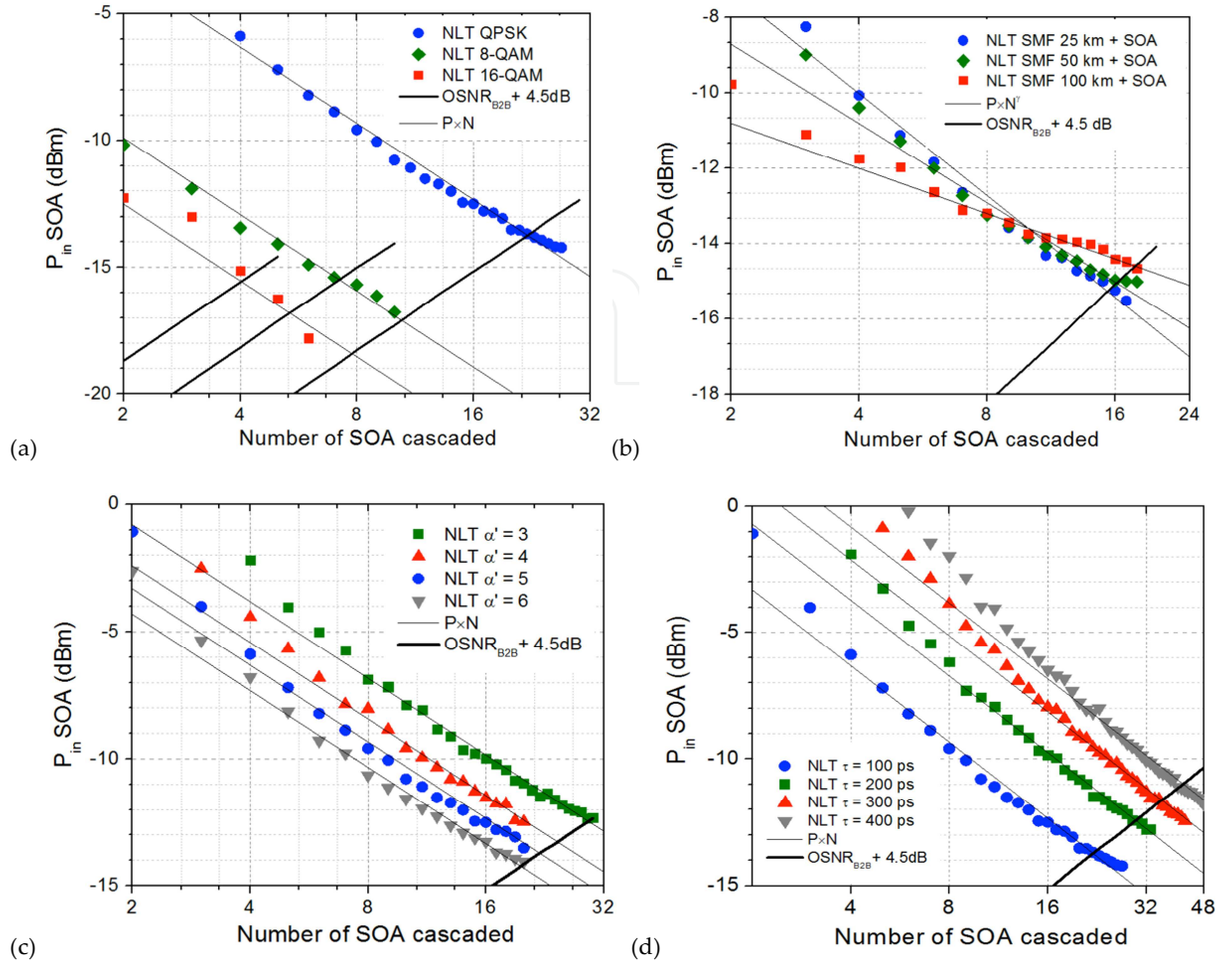

Figure 15. NLT and OSNR limits versus number of cascaded SOAs (a) for QPSK, 8-QAM, 16-QAM formats of signal, (b) for QPSK signal and 25 km (γ = 0.9), 50 km (γ = 0.7), and 100 km (γ = 0.4) SMF inter-SOA spans, (c) for QPSK signal and SOA line-width factor 3, 4, 5, 6, and (d) for QPSK signal and SOA carriers' lifetime 100 ps, 200 ps, 300 ps, and 400 ps.

higher input power needs to be injected into the SOA. However, the nonlinear behavior of SOA limits the maximum input optical power. QPSK, 8-QAM, and 16-QAM optical signals are studied in Figure 15(a). The NLT slope is the same for all three modulation formats. The impact of the extinction ratio explains the large shift from QPSK to M-QAMs due to amplitude level changes (as previously explained for OOK signals). Different fiber span lengths are simulated in Figure 15(b). We use the general IP law as previously detailed. The noise dependence on span input cumulated CD and uncorrelated noise contributions from span to span due to the large relative span input cumulated CD [71] induces such that γ is close to 0.67 for 100-km-long CD-unmanaged 100 Gb/s systems. The impact of the line-width enhancement factor and the carriers' lifetime of the SOA on signal degradation are presented in Figure 15(c) and Figure 15(d), respectively. We simulate a cascade of SOAs with different line-width enhancement factor from 3 to 6 and carrier lifetime from 100 ps to 400 ps (again with a 100 Gb/s QPSK signal). We observe the same slope for all the cases and apply a common $P_{in} \times N$ convergence rule to demonstrate identical nature of the penalties [69]. As the line-width enhancement factor variations are less influential for high-degree M-QAM formats as con-

cluded in reference [72], SOA with shorter carrier lifetime should be chosen for complex modulation signals.

4.2. Experimental evaluation

In this section, we confront the models with experimental results obtained with conventional, transmission SOAs. For the direct detection experiment, the ring consists of a repetition of four times a pattern made of a transmission link followed by an OPS/OSS node [6]. Each transmission link is composed of 50 km of standard SMF followed by dispersion compensating fiber to provide full chromatic dispersion compensation, in between EDFAs; 2-μs-long data packets with (2^{31}–1)-long PRBS are used at 1549.3 nm. Our burst-mode receiver was designed to operate at 10 Gbit/s including 7% forward error correction (FEC) and protocol overhead. BER measurements are done using a standard error counter. Before entering the burst-mode receiver, the signal performance is artificially degraded with a variable optical attenuator or a noise-loading device. The concept of the experimental setup for the coherent experiment is depicted in Figure 16. We use a dual-polarization I/Q modulator for the coherent detection experiments. Four digital-to-analog converters were used to drive the modulator, generating PDM signals at 28 Gbaud with diverse modulation formats: QPSK, 8-, and 16-QAM. All signals are based on PRBS of length 2^{15}–1 bits. After traversing a polarization scrambler, the light enters into a recirculating loop emulating the propagation through many optical nodes. In order to emulate such nodes, an optical packet blocker is built with two wavelength-selective switches working as wavelength (de)multiplexer and a commercial SOA as optical gate and amplifier with 11 dB optical gain. A variable optical attenuator is used to control the launching power into the loop containing 25 km of SMF, SOA, and EDFA. Finally, optical signals are detected using a coherent mixer and four pairs of balanced photodiodes connected to a 20-GHz bandwidth oscilloscope working at 40 GS/s. All measured waveforms were processed offline [73].

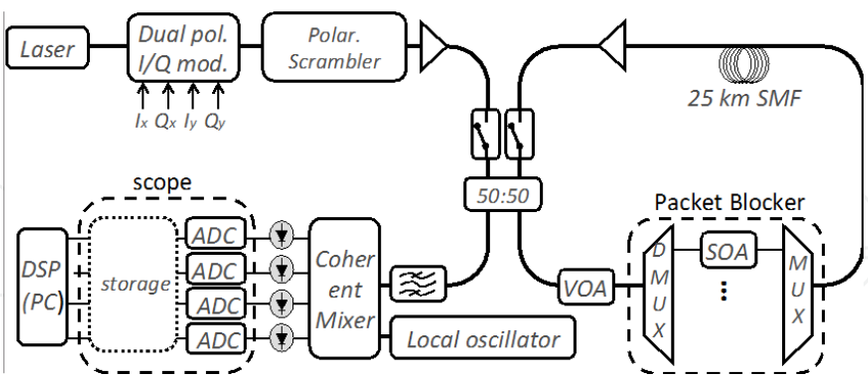

Figure 16. Experimental recirculation optical loop for high data rate coherent packet-switched network.

4.2.1. NRZ-OOK optical packet experiments

In the back-to-back experiment, the required OSNR yielding 10^{-3} BER was found at 11 dB, corresponding to an extinction ratio of r_0 = 13.5 dB from equation (16). We measured the OSNR penalties at 10^{-3} BER arising from a series of SOAs versus the IP. Up to four devices are

http://dx.doi.org/10.5772/61990

cascaded. Their input optical power levels are varied over a large operation range, from −20 dBm to 7 dBm. We report the results in Figure 17(a). It can be observed that the plots gather almost on a single curve. This curve is found to match very well the predictions from the analytical model proposed in Section 3.3.1, when the data of Figure 8(a) are used as input parameters. Based on Figure 13(a) and Figure 17(a), we restrict the experimental measurements to only one SOA. The NLT can be easily derived, at −3 dBm. Besides, we characterized NF of our transmission SOA, which was found to be 8 dB. RSOAs share the same fundamental building block as SOAs; therefore, we will assume that all the above considerations also apply to RSOAs. Hence, we just need to characterize a single device in order to predict system performance in a multi-device network. We report the OSNR penalty versus integrated power [in Figure 17(b)] after one single module and derive the NLTs. We first inserted an RSOA device, optimized for access networks (G = 24 dB, P_{sat} = 6.5 dBm) [74]. The distortions due to nonlinearities were found prohibitively high for our applications. The measured NLT does not exceed −17 dBm, that is, 14 dB worse than the transmission SOA. Then, we tested a specific RSOA with a reduced gain in order to contain nonlinearities (G = 7 dB, P_{sat} = 4.1 dBm). With these parameters, the NLT is increased to −3 dBm, similar to the transmission SOA, as reported in Figure 17(b). From a noise point of view, both RSOA devices exhibit a noise figure of 11 dB, that is, 3 dB larger than for the transmission SOA. The analytical model of Section 3.3.1 has been proposed to predict the level of distortions versus optical power. Therefore, it can also be used to derive the optical power, which guarantees a given level of distortions (i.e., a given BER). The evolution range of (R)SOA input powers with respect to the maximum number of cascaded nodes is presented in Figure 17(c) for SOA and RSOA devices. As described in Section 4.1.2, the maximum number of cascaded SOA could be found when the nonlinear and the ASE limits intersect. RSOAs specially designed for access network show high nonlinearity, which limits the maximum number of cascaded devices to five with 10 Gbit/s NRZ signal. With the RSOA of reduced optical gain, 26 devices can be cascaded. Optimized SOA with high saturation power allows even higher number of cascaded devices (up to 37).

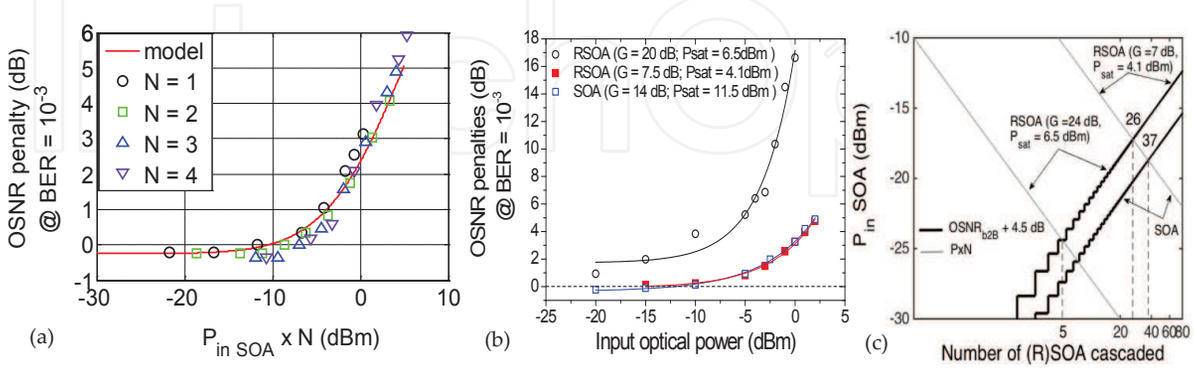

Figure 17. (a) Penalty for various configurations of SOA cascades. (b) Measured penalties caused by three types of (R)SOAs (one device per configuration, no cascade). (c) Number of cascades for SOAs and RSOAs devices for 10 Gbit/s OOK-NRZ signals.

4.2.2. PDM-QPSK, PDM-8QAM, and PDM-16QAM optical packets experiment

In this section, the impairments produced in coherent signals when traversing a long cascade of SOAs are presented following the work done in reference [73]. The setup on Figure 16 allows for a full characterization of the performance in a network comprising unlimited number of SOAs. Moreover, the capability of controlling the input power into an SOA permits to determine the impact of traversing such device when working in different regimes. Finally, coherent detection enables to study the evolution of the whole optical field along the cascade of SOAs.

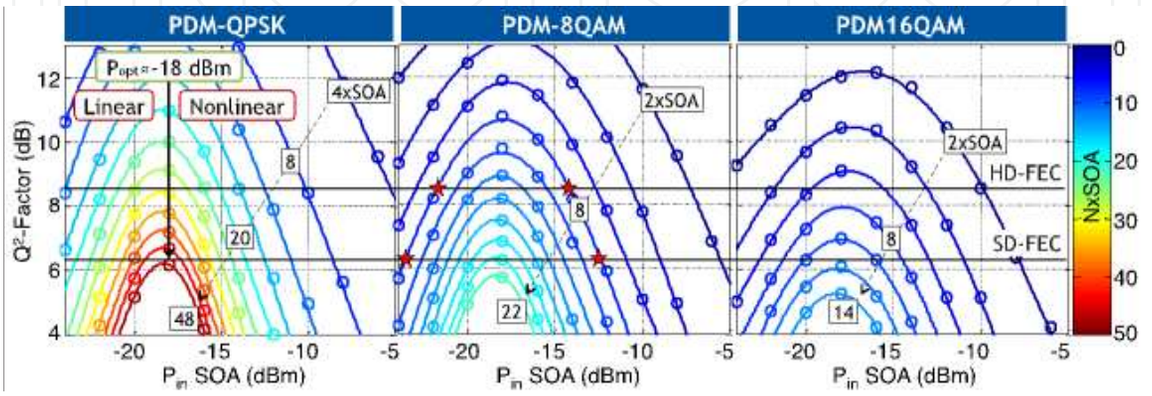

Figure 18. Q^2-Factor versus input power in the SOA evaluated along the SOA cascade for different modulation formats.

Figure 18 depicts the performance of the different modulation formats when traversing the SOA cascade under different working regimes of such device. In such graphs, each curve represents the Q^2-Factor as a function of the power inserted into the SOA (P_{inSOA}) after traversing *N* times through the device (see color scale and boxed numbering). Using a power range between −24 and 0 dBm, such results describe most realistic ranges of operation of the SOA. As can be seen, each curve shows a maximum performance when setting an optimal $P_{inSOA} \approx -18$ dBm (P_{opt}) for most cases, corresponding to the P_{inSOA} at which the SOA gain starts saturating. Therefore, such input optical power distinguishes the linear regime ($P_{inSOA} < P_{opt}$) from the nonlinear regime ($P_{inSOA} > P_{opt}$). As described in Section 4.1.1, the NLT can be extracted from the OSNR penalty depending on the IP. We compare the experimental data with the simulations proposed in Section 4.1.2. We use the 1.76-dB OSNR penalty to assess the NLT after the cascade of SOAs. We use a 28-Gbaud NRZ optical signal based on PRBS of length 2^{15}–1 bits as in the experiment. Concerning the SOA model, we use the provided parameters corresponding to our commercial SOA used in this experiment (optical gain of 11 dB, saturation power of 13 dBm, and NF of 6.9 dB). Then, we adjust the carrier lifetime as well as the alpha factor, which are not provided. We use a recombination carrier lifetime of 100 ps and high alpha factor of 15 dB in order to increase the impact of the amplitude and phase deviations. The OSNR penalty versus the IP is presented in Figures 19(a) and (b) for PDM-8QAM and PDM-16QAM signals, respectively. Good matching is obtained, however, at the expense of the alpha factor. We believe such difference is due to the non-ideal signal generation/detection of our optical setup.

http://dx.doi.org/10.5772/61990

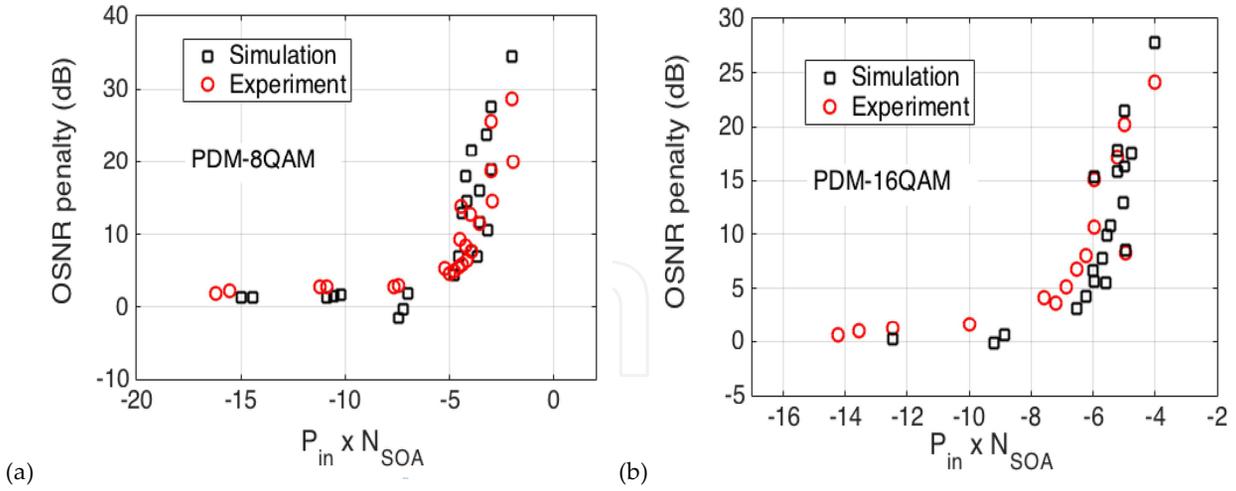

Figure 19. Modeled and experimental OSNR penalty depending on $N \times P_{\text{in SOA}}$ (a) for PDM-8QAM and (b) PDM-16QAM.

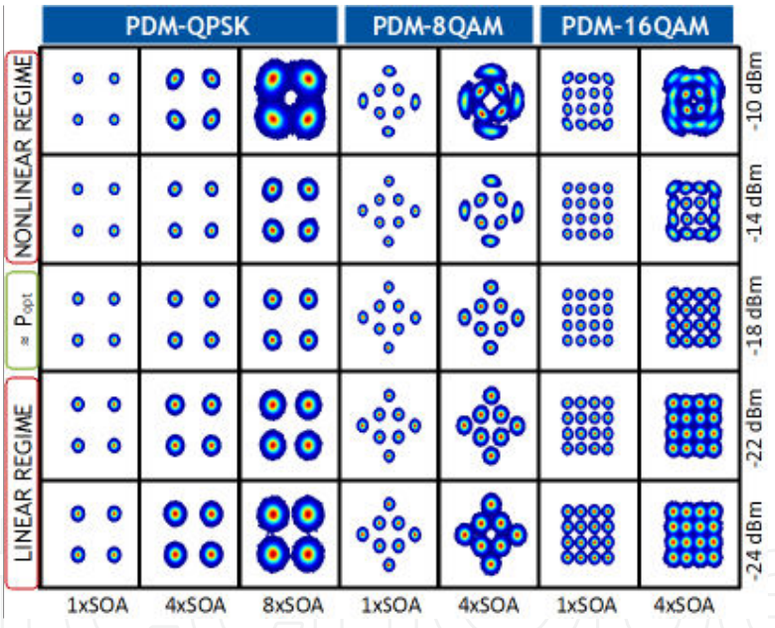

Figure 20. Exemplary constellations of recovered signals along the SOA cascade for different working regimes.

In Figure 20, we depict the recovered exemplary constellations after traversing several SOAs for different operating regimes. Irrespective of the modulation format, one can clearly notice that, in the linear regime, the constellations degrade isotropically along the cascade, which denotes the ASE noise being the major impairment. On the other hand, in the nonlinear regime, constellations evolve differently. In such regime, one can already observe by visual inspection that the phase noise grows faster than the amplitude noise, indicating the predominance of self-phase modulation as main distortion. One can notice that such impairment is even more critical for QAM signaling. This is due to greater amplitude oscillations of such modulation

formats (due to the modulation format itself) with respect to QPSK, which amplitude only changes during inter-symbol transitions. It is important to remember that amplitude modulation induces a change of the SOA gain (when being under saturation), leading to SPM.

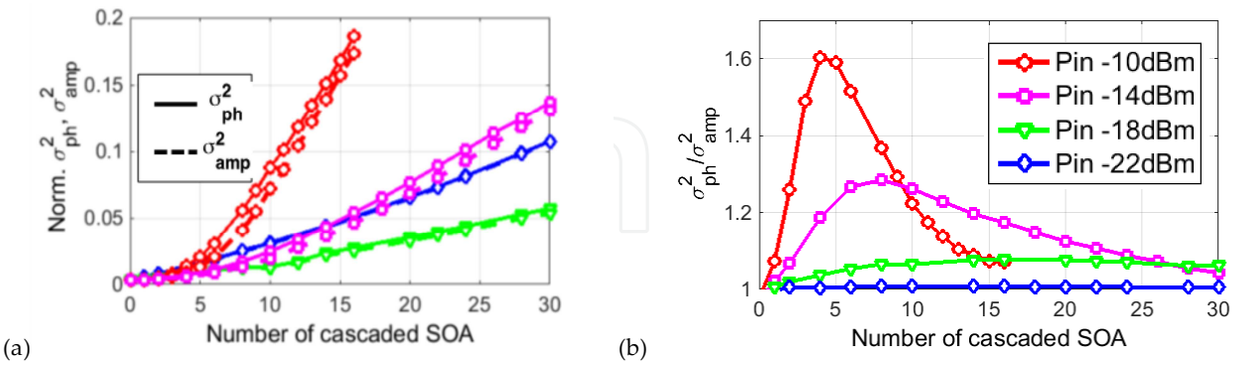

Figure 21. (a) Normalized variances and (b) phase-amplitude variance ratio evolution along the SOA cascade.

In order to study the noise evolution along the cascade, the phase and amplitude variances (σ_{ph}^2 and σ_{amp}^2, respectively) for several P_{inSOA} are calculated for the QPSK signal [see Figure 21(a)]. When the input optical power is optimum ($P_{inSOA} = -18$ dBm as shown in Figure 18), the slope of the variances (σ_{ph}^2 and σ_{amp}^2) as a function of the number of cascaded SOAs is minimum. Moving away from such optimum power leads to an increase of the slope, thereby leading to a faster degradation of the performances (as seen in Figure 18). In Figure 21(b), the ratio $\sigma_{ph}^2/\sigma_{amp}^2$ is plotted for the same conditions as in Figure 21(a). One can denote the increase of the phase with respect to the amplitude variance at high-input optical power. However, on the one hand, along the cascade, the constellation becomes more isotropic, meaning that σ_{amp}^2 tends to approach σ_{ph}^2 (see QPSK constellations at $P_{inSOA} = -10$ dBm in Figure 20 for visual aid). On the other hand, in the linear regime, all constellations remain mainly isotropic (see $P_{inSOA} = -22$ dBm in Figure 20).

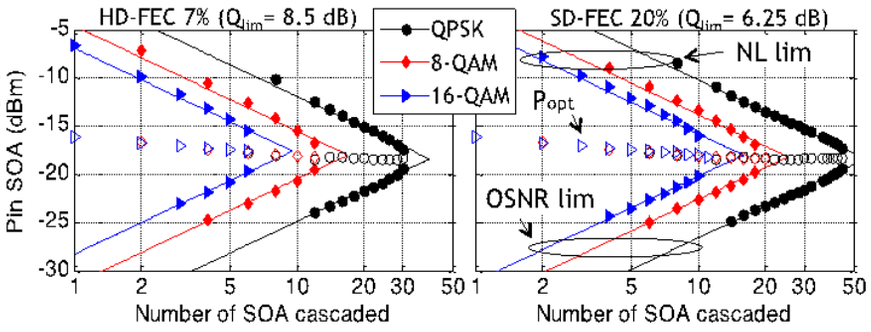

Figure 22. Experimental values (markers) and linear fit (lines) of nonlinear and OSNR limits that meet HD- and SD-FEC requirements, and optimal power as a function of the number of cascaded SOAs.

The degradation observed due to the accumulation of distortions induced by the SOAs will limit the reach of the transmitted signals. Such reach depends on the forward error correction (FEC) scheme used to recover the signals. Typically, two FEC schemes might be applied: hard-

decision (HD-) FEC with 7% overhead or soft-decision (SD-) FEC with 20% overhead, which requires Q^2-factors of 8.5 and 6.25 dB, respectively, to properly recover the information.

The nonlinear limit as well as the OSNR limit could be derived from the OSNR penalty versus the IP as presented in Figures 19(a) and (b). In this experiment, we directly look at the Q^2-factor when moving below the considered FEC limits (8.5 and 6.25 dB) at a given input SOA power and extract the maximum number of cascaded SOA (see stars in Figure 18 as example). As described in Section 4.2.1, the largest count of cascadable SOAs is obtained at the optimal trade-off between distortions and noise, when nonlinear and OSNR limits cross. The results are presented in Figure 22 for both FECs. The empty markers show the evolution of P_{opt} in order to guarantee the maximum number of cascaded devices. It increases from −16 dBm to around −18 dBm for all formats. One can observe that a large reach of up to 44, 20, and 11 nodes (1100, 500, and 275 km) can be achieved with QPSK, 8-, and 16-QAM signals, respectively, using SD-FEC (30, 12, and 6 SOAs using HD-FEC). More details of this experiment are presented in reference [73]. One can observe that all fits (straight lines) match the experimental results, leading to a simple linear law that identifies the possible operational SOA range assuring performance for different modulations formats and FEC schemes. Design rules for SOA-based network could be derived as described by the first-order linear IP law (Section 4.1.1); however, such linear behavior is obtained in some specific scenario and an extra coefficient is to be added (general IP law) if different fiber length is considered, for example (as described by simulations in Section 4.1.2). Therefore, controlling the optical power variation between optical packets is crucial in order to operate the network in optimum conditions. Several techniques have been proposed in order to tackle this issue, such as employing an all-optical power equalization scheme based on two SOAs [75], hybrid optoelectronics control configuration [76,77] and dynamic gain control of SOAs [78,79]. We experimentally assess the system advantages of distributed power equalization scheme based on an automatic gain control SOA in a WDM packet-switched ring network composed of five cascaded network sections and show that error floor could be removed. More details can be found in reference [80].

5. Conclusion

Optical packet switching is a promising approach for highly efficient and dynamic optical networks allowing sub-wavelength networking directly at the optical layer. Furthermore, the reductions of optoelectronic conversion translate into energy savings. First, we reviewed the advantages of optical packet-switched network against circuit-switched, electronic packet, and optical transport networks. Then, we focused on the slot blocker implementation. This building block is a key enabler for efficient wavelength utilization. One potential candidate to fulfill the logic gate functionality is the SOA, due to its large optical bandwidth, low switching time, and high optical gain. In this chapter, we focused on the impact of SOA in a large cascade of OSS nodes. The SOA theory was discussed and we underlined several physical mechanisms that are responsible for the signal degradation. Thus, the SOA limits the signal reach due to the OSNR degradation by ASE and nonlinear distortions (mainly extinction ratio degradation and self-phase modulation) in the passing signal. We proposed an analytical model enabling to characterize the accumulation of SOA-based nonlinearities over an OOK-NRZ signal and

experimentally assessed its accuracy. Different types of (R)SOA devices are studied and a convergence rule (IP law: $P_{in} \times N$) is proposed paving the way to new design rules for SOA-based OSS network (up to 37 SOA-based nodes could be cascaded). Then, by the means of numerical simulations, we assessed the impact of the cascade of SOAs on higher modulation formats such as QPSK, 8-QAM, and 16-QAM. We studied the role of SOA parameters in the amplitude and phase integrity of the optical signal. We verified the applicability of the IP law to the accumulation of nonlinearities in SOA cascade with QPSK and M-QAM signals and proposed modified IP rule $P_{in} \times N^{\gamma}$ for spans including fibers and SOAs. Finally, we experimentally studied a large cascade of SOA with several high-order modulation formats (PDM-QPSK, 8-, and 16-QAM signals at 28 GBaud). Design rules could be extracted in order to guarantee error-free operation after different FECs. Long reach of 44, 20, and 11 SOA-based nodes has been achieved by PDM-QPSK, -8QAM, and -16QAM signals at 28 GBaud, respectively, thus establishing SOA as a promising candidate for coherent optical slot-switched networks.

Author details

Guilhem de Valicourt[1*], Miquel Angel Mestre Adrover[2], Nikolay D. Moroz[3] and Yvan Pointurier[2]

*Address all correspondence to: devalicourt@bell-labs.com

1 Bell Labs, Alcatel-Lucent, Holmdel, New Jersey, USA

2 Alcatel-Lucent Bell Labs France, Nozay, France

3 T8 Company, Moscow, Russia

References

[1] P. Winzer, "Beyond 100G Ethernet," IEEE Communications Magazine, vol. 48, no. 7, pp. 26–30, July 2010.

[2] G. Raybon, et al., "High Symbol Rate Transmission Systems for Data Rates above 400 Gb/s Using ETDM Transmitters and Receivers," in Proc. ECOC'14, Tu.3.3.5, Cannes, France, 2014.

[3] R. Rios-Müller, et al., "1-Terabit/s Net Data-Rate Transceiver Based on Single-Carrier Nyquist-Shaped 124 GBaud PDM-32QAM," in Proc. OFC'15, Th5B.1, Los Angeles, USA, 2015.

[4] Alcatel-Lucent Bell Labs, "Metro network traffic growth: an architecture impact study," Strategic white paper, 2013.

[5] Y. Pointurier, et al., "Dimensioning and Energy Efficiency of Optical Metro Rings," in Proc. ONDM 2012, Colchester, 2012.

[6] D. Chiaroni, et al., "Packet OADMs for the next generation of ring networks," Bell Labs Technical Journal, vol. 14, no. 4, pp. 265–283, Winter 2010.

[7] H.-W. Chen, et al., "Forty Gb/s hybrid silicon Mach-Zehnder modulator with low chirp," Optics Express, vol. 19, no. 2, pp. 1455–1460, 2011.

[8] W. Zhang, et al., "Broadband silicon photonic packet-switching node for large-scale computing systems," IEEE Photonics Technology Letters, vol. 24, no. 8, pp. 688–690, 2012.

[9] H. Nishi, et al., "Monolithic Integration of a Silica-based Arrayed Waveguide Grating Filter and Silicon Variable Optical Attenuators based on p-i-n Carrier-Injection Structures," in Proc. ECOC 2010, We.8.E.3, Torino, 2010.

[10] G. de Valicourt, et al., "Monolithic Integrated Silicon-based Slot-Blocker for Packet-Switched Networks," in Proc. ECOC'14, We.3.5.5, Cannes, France, 2014.

[11] G. de Valicourt, et al., "Monolithic Integrated Reflective Polarization Diversity SOI-based Slot-Blocker for Fast Reconfigurable 128 Gb/s and 256 Gb/s Optical Networks," in Proc. ECOC'15, Tu.3.5.4, Valencia, Spain, 2015.

[12] A. Garreau, et al., "10 Gbit/s Drop and Continue Colorless Operation of a 1.5μm AlGaInAs Reflective Amplified Electroabsorption Modulator," in Proc. ECOC'06, We. 1.6.5, Cannes, France, Sep. 2006.

[13] G. de Valicourt, et al., "Reflective Packet Add-Drop Multiplexer based on Modulation Format Agnostic and Low Cost Optical Gate," in Proc. ECOC'12, We.2.B.5, Amsterdam, Netherlands, 2012.

[14] G. de Valicourt, et al., "A next-generation optical packet-switching node based on hybrid III-V/silicon optical gates," IEEE Photonics Technology Letters, vol. 26, no. 7, pp. 678–681, April 1, 2014.

[15] Y. Pointurier, et al., "Dimensioning and energy efficiency of multi-rate metro networks," IEEE/OSA Journal of Lightwave Technology, vol. 30, no. 22, pp. 3552–3564, 15 November 2012.

[16] Intune Networks, http://www.intunenetworks.com/.

[17] L. Dittmann, et al., "The European IST project DAVID: a viable approach toward optical packet switching," IEEE Journal of Selected Areas in Communication, vol. 21, no. 7, pp. 1026–1040, September 2003.

[18] M.C. Yuang, et al., "HOPSMAN: an experimental testbed system for a 10-Gb/s optical packet-switched WDM metro ring network," IEEE Communications Magazine, vol. 46, no. 7, pp. 158–166, July 2008.

[19] J. Dunne, et al., "Optical Packet Switch and Transport: A New Metro Platform to Reduce Costs and Power by 50% to 75% While Simultaneously Increasing Deterministic Performance Levels," in Proc. BROADNETS, Madrid, Spain, September 2009.

[20] N. Deng, et al., "A Novel Optical Burst Ring Network with Optical-Layer Aggregation and Flexible Bandwidth Provisioning," in Proc. OFC, OThR5, Los Angeles, CA, March 2011.

[21] J.E. Simsarian, et al., "Fast-tuning coherent burst-mode receiver for metropolitan networks," IEEE Photonics Technology Letters, vol. 26, no. 8, pp. 813–816, April 2014.

[22] I. Widjaja, et al., "Light core and intelligent edge for a flexible, thin-layered, and cost-effective optical transport network," IEEE Communications Magazine, vol. 41, no. 5, pp. S30–S36, May 2003.

[23] R. Luijten, et al., "Optical Interconnection Networks: The OSMOSIS Project," in Proc IEEE LEOS 2004, Rio Grande, Puerto Rico, November 2004.

[24] A. Stavdas, et al., "Dynamic CANON: a scalable multidomain core network," IEEE Communications Magazine, vol. 46, no. 6, pp. 138–144, June 2008.

[25] K.-I. Kitayama, et al., "Torus-topology Data Centre Network based on optical packet/agile circuit switching with intelligent flow management," IEEE/OSA Journal of Lightwave Technology, vol. 29, no. 5, pp. 1063–1071, 1 March 2015.

[26] N.G. Basov, et al., "Production of negative-temperature states in p–n junctions of degenerate semiconductors," Soviet Physics, Journal of Experimental and Theoretical Physics, vol. 13, no. 6, pp. 1320–1321, 1961.

[27] M.G.A. Bernard and G. Duraffourg, "Laser conditions in semiconductors," Physica Status Solidi, vol. 1, no. 7, pp. 699–703, 1961.

[28] R.N. Hall, et al., "Coherent light emission from GaAs junctions," Physical Review Letters, vol. 9, no. 9, pp. 366–368, 1962.

[29] M.I. Nathan, et al., "Stimulated emission of radiation from GaAs p-n junctions," Applied Physics Letters, vol. 1, no. 3, pp. 62–64, 1962.

[30] H. Kroemer, "A proposed class of heterojunction injection lasers," Proceedings of the IEEE, vol. 51, no. 12, pp. 1782–1783, 1963.

[31] H. Kressel and H. Nelson, "Close-confinement gallium arsenide P-N junction lasers with reduced optical loss at room temperature," RCA Review, vol. 30, pp. 106–113, 1969.

[32] P.G. Kryukov and V.S. Letokhov, "Propagation of a light pulse in a resonantly amplifying (absorbing) medium," Soviet Physics Uspekhi, vol. 12, no. 5, pp. 641–672, March 1970.

[33] L.W. Casperson, "Threshold characteristics of mirrorless lasers," Journal of Applied Physics, vol. 48, no. 1, pp. 256–262, January 1977.

[34] G. Zeidler and D. Schicetanz, "Use of laser amplifiers in glass fibre communication systems," Radio and Electronic Engineer, vol. 43, no. 11, pp. 675–682, 1973.

[35] S.D. Personick, "Applications for quantum amplifier in simple digital optical communication systems," Bell System Technical Journal, vol. 52, no. 1, pp. 117–133, 1973.

[36] J.C. Simon, "Polarisation characteristics of a travelling-wave-type semiconductor laser amplifier," Electronics Letters, vol. 18, no. 11, pp. 438–439, May 1982.

[37] T. Saitoh and T. Mukai, "A Low Noise 1.5 μm GaInAsP Traveling-Wave Optical Amplifier with High Saturation Output Power," in ISLC, PD-5, Kanazawa, Japan, 1986.

[38] Y. Yamamoto, "Charasteristics of AlGaAs Fabry-Perot cavity type laser amplifiers," Journal of Quantum Electronics, vol. 16, no. 10, pp. 1047–1052, 1980.

[39] J.C. Simon, "GaInAsP semiconductor laser amplifiers for single-mode fibre communications," Journal of Lightwave Technology, vol. LT-5, no. 9, pp. 1286–1295, 1987.

[40] N.A. Olsson, et al., "Polarization-independent optical amplifier with buried facets," Electronics Letters, vol. 25, no. 16, pp. 1048–1049, 1989.

[41] D.M. Atkin and M.J. Adams, "Optical switching in the twin-guide travelling-wave laser amplifier," IEE Proceedings Journal, vol. 140, no. 5, pp. 296–300, October 1993.

[42] T. Kirihara, et al., "Lossless and low-crosstalk characteristics in an InP-based 4x4 optical switch with integrated single-stage optical amplifiers," Photonics Technology Letters, vol. 6, no. 2, pp. 218–221, February 1994.

[43] I. Valiente, et al., "Theoretical analysis of semiconductor optical amplifier wavelength shifter," Electronics Letters, vol. 29, no. 5, pp. 502–503, March 1993.

[44] T. Durhuus, et al., "All-optical wavelength conversion by semiconductor optical amplifiers," Journal of Lightwave Technology, vol. 14, no. 6, pp. 942–954, June 1996.

[45] L. Gillner, "Modulation properties of a near travelling-wave semiconductor laser amplifier," IEE Proceedings Journal, vol. 139, no. 5, pp. 331–338, October 1992.

[46] A.C. Labrujere, et al., "Phase modulation and optical switching by semiconductor laser amplifier," , ThC4, Technical Digest Series Optical Society of America, Washington, pp. 138–141, 1991.

[47] R. Schnabel, et al., "All Optical AND Gate Using Femtosecond Non-Linear Gain Dynamics in Semiconductor Optical Amplifiers," in Proc. ECOC'93, Montreux, Switzerland, pp. 133–136, September 1993.

[48] C. Joergensen, et al., "4 Gb/s Optical wavelength conversion using semiconductor optical amplifiers," Photonics Technology Letters, vol. 5, no. 6, pp. 657–660, June 1993.

[49] S. Kawanishi, et al., "Ultrahigh-speed phaselocked-loop-type clock recovery circuit using a travelling-wave laser diode amplifier as a 50 GHz phase detector," Electronics Letters, vol. 29, no. 19, pp. 1714-1716, September 1993.

[50] J. Leuthold, et al., "An All-Optical Grooming Switch with Regenerative Capabilities," in Proc. ICTON, Azores, Portugal, pp. 1–4, 2009.

[51] A.H. Gnauck, et al., "10 –Gb/s 360-km transmission over dispersive fiber using mid-system spectral inversion," Photonics Technology Letters, vol. 5, no. 6, pp. 663-666, June 1993.

[52] P.Y. Cortès, et al., "Below 0.3 dB Polarisation Penalty in 10 Gbit/s Directly Modulated DFB Signal Over 160 Km using Mid-Span Spectral Inversion in a Semiconductor Optical Amplifier," in proc. ECOC'95, Brussels, Belgium, pp. 267–270, September 1995.

[53] L. Noel, et al., "Four WDM channel NRZ to RZ format conversion using a single semiconductor laser amplifier," Electronics Letters, vol. 31, no. 4, pp. 277–278, February 1995.

[54] G.P. Agrawal and A.N. Olsson. Self-phase modulation and spectral broadening of optical pulses in semiconductor laser amplifiers. IEEE Journal of Quantum Electronics. vol. 25, no. 11, pp. 2297-2306, 1989. DOI: 10.1109/3.42059.

[55] G.P. Agrawal, "Fiber Optics Communication Systems," Wiley Interscience, New York, 1992.

[56] M. Shtaif, et al., "Noise spectra of semiconductor optical amplifiers: relation between semiclassical and quantum descriptions," Journal of Quantum Electronics, vol. 34, no. 5, pp. 869-878, 1998.

[57] R. Brenot, et al., "Experimental Study of the Impact of Optical Confinement on Saturation Effects in SOA," in Proc. OFC 2005, OME50, Anaheim, CA, USA, March 2005.

[58] G. de Valicourt, et al., "10Gbit/s Modulation of Reflective SOA without Any Electronic Processing," in Proc. OFC'11, OThT2, Los Angeles, USA, 2011.

[59] G. de Valicourt, Chapter 1: "Next generation of Optical Access Network based on Reflective-SOA," Book: "Selected Topics on Optical Amplifiers in Present Scenario," Dr. Sisir Garai (Ed.), ISBN: 978-953-51-0391-2, InTech, (invited), 2012.

[60] C.H. Henry, "Theory of the linewidth of semiconductor lasers," IEEE Journal of Quantum Electronics, vol. 18, no. 2, pp. 259–264, 1982. DOI: 10.1109/JQE.1982.1071522.

[61] F. Koyama and K. Iga, "Frequency chirping in external modulators," Journal of Lightwave Technology, vol. 6, no. 1, pp. 87–93, January 1988.

[62] T. Watanabe, et al., "Transmission performance of chirp-controlled signal by using semiconductor optical amplifier," Journal of Lightwave Technology, vol. 18, no. 8, pp. 1069–1077, August 2000.

[63] G. de Valicourt, et al., “Cascadability of optical packet-switching nodes based on (R)SOA devices,” IEEE Photonics Technology Letters, vol. 25, no. 24, pp. 2389–2392, December 15, 2013.

[64] J.-C. Antona, et al., “Physical design and performance estimation of heterogeneous optical transmission systems,” Comptes Rendus Physique, vol. 9, no. 9–10, pp. 963-984, November 2008.

[65] D. Cassioli, et al., “A time-domain computer simulator of the nonlinear response of semiconductor optical amplifiers,” IEEE Journal of Quantum Electronics, vol. 36, no. 9, pp. 1072–1080, 2000.

[66] A. Ghazisaeidi, et al., “Bit patterning in SOAs: statistical characterization through multicanonical Monte Carlo simulations,” IEEE Journal of Quantum Electronics, vol. 46, no. 4, pp. 570–578, 2010. DOI: 10.1109/JQE.2009.2029545.

[67] P. Borri, et al., “Spectral hole-burning and carrier-heating dynamics in InGaAs quantum-dot amplifiers,” IEEE Journal of Selected Topics in Quantum Electronics, vol. 6, no. 3, pp. 544–551, 2000. DOI: 10.1109/2944.865110.

[68] A. Ghazisaeidi and L.A. Rusch, “On the efficiency of digital back-propagation for mitigating SOA-induced nonlinear impairments,” Journal of Lightwave Technology, vol. 29, no. 21, pp. 3331–3339, 2011.

[69] N.D. Moroz, et al., "On accumulated signal degradation in a cascade of semiconductor optical amplifiers," Journal of Physics: Conference Series, 584 012008, 2015.

[70] E. Grellier and A. Bononi, “Quality parameter for coherent transmissions with Gaussian-distributed nonlinear noise,” Optics Express, vol. 19, no. 13, pp. 12781–12788, June 2011.

[71] F. Vacondio, et al., “On nonlinear distortions of highly dispersive optical coherent systems,” Optics Express, vol. 20, no. 2, pp. 1022–1032, January 2012.

[72] R. Bonk, et al., “Linear semiconductor optical amplifiers for amplification of advanced modulation formats,” Optics Express, vol. 20, no. 9, pp. 9657– 9672, April 2012.

[73] M.A. Mestre, et al., "On the SOA Cascadability and Design Rules for Optical Packet-Switched Networks," Optical Fiber Communication Conference, OSA Technical Digest (online) (Optical Society of America, 2015), paper Th2A.2.

[74] G. de Valicourt, et al., “High gain (30 dB) and High saturation power (11dBm) RSOA devices as colourless ONU sources in long reach hybrid WDM/TDM -PON architecture,” IEEE Photonics Technology Letters, vol. 22, no. 3, pp. 191–193, Feb. 2010.

[75] S. Pato, et al., "On Using All-Optical Burst-Mode power Equalization in Converged Metro-Access Networks," ICTON 2009, We.B2.1, 2009

[76] H. Wessing, et al., "Combining Control Electronics with SOA to Equalize Packet-to-Packet Power Variations for Optical 3R Regeneration in Optical Networks at 10 Gbit/s," OFC'2004, paper WD2, 2004.

[77] A.V. Tran, et al., "Optical Packet Power Equalization with Large Dynamic Range using Controlled Gain-Clamped SOA," OFC 2005, OME46, 2005.

[78] N. Cheng, et al., "Long Reach Passive Optical Networks with Adaptive Power Equalization using Semiconductor Optical amplifiers," OSA/ACP'2009, paper FS4, 2009.

[79] Y. Kai, et al., "MSA Compatible Size, Dual-channel Fast Automatic Level Controlled SOA substems fro Optical Packet and PON signals," in Proc. ECOC'2011, Mo.2.A.2, 2011.

[80] G. de Valicourt, et al., "Distributed fast optical packet power equalization for efficient WDM packet switched networks," in Proc. ECOC'12, Tu.3.A.4, Amsterdam, Netherlands, 2012.